












## The Luminosity Phase Space of Galactic and Extragalactic X-ray Transients Out to Intermediate Redshifts

AVA POLZIN <sup>1</sup>, RAFFAELLA MARGUTTI <sup>2,3</sup>, DEANNE L. COPPEJANS <sup>4,5</sup>, KATIE AUCHETTL <sup>6,7,8</sup>, KIM L. PAGE <sup>9</sup>,  
GEORGIOS VASILOPOULOS <sup>10,11</sup>, JOE S. BRIGHT <sup>12</sup>, PAOLO ESPOSITO <sup>13,14</sup>, PETER K. G. WILLIAMS <sup>15,16</sup>,  
KOJI MUKAI <sup>17,18</sup> AND EDO BERGER <sup>15</sup>

<sup>1</sup>*Department of Astronomy and Astrophysics, The University of Chicago, Chicago, IL 60637, USA*

<sup>2</sup>*Department of Astronomy, University of California, Berkeley, CA, 94720, USA*

<sup>3</sup>*Department of Physics, University of California, Berkeley, CA, 94720, USA*

<sup>4</sup>*Department of Physics, University of Warwick, Gibbet Hill Road, Coventry CV4 7AL, UK*

<sup>5</sup>*Department of Physics & Astronomy and Center for Interdisciplinary Exploration and Research in Astrophysics, Northwestern University, Evanston, IL, 60208, USA*

<sup>6</sup>*School of Physics, The University of Melbourne, Parkville, VIC 3010, Australia*

<sup>7</sup>*ARC Centre of Excellence for All Sky Astrophysics in 3 Dimensions (ASTRO 3D)*

<sup>8</sup>*Department of Astronomy and Astrophysics, University of California, Santa Cruz, CA 95064, USA*

<sup>9</sup>*School of Physics & Astronomy, University of Leicester, Leicester LE1 7RH, UK*

<sup>10</sup>*Université de Strasbourg, CNRS, Observatoire astronomique de Strasbourg, UMR 7550, F-67000 Strasbourg, France*

<sup>11</sup>*Department of Physics, National and Kapodistrian University of Athens, University Campus Zografos, GR 15784, Athens, Greece*

<sup>12</sup>*Astrophysics, Department of Physics, University of Oxford, Keble Road, Oxford OX1 3RH, UK*

<sup>13</sup>*Scuola Universitaria Superiore IUSS Pavia, Palazzo del Broletto, piazza della Vittoria 15, 27100 Pavia, Italy*

<sup>14</sup>*INAF–Istituto di Astrofisica Spaziale e Fisica Cosmica di Milano, Via A. Corti 12, 20133 Milano, Italy*

<sup>15</sup>*Center for Astrophysics | Harvard & Smithsonian, 60 Garden Street, Cambridge, MA 02138-1516, USA*

<sup>16</sup>*American Astronomical Society, 1667 K Street NW, Suite 800, Washington, DC, 20006, USA*

<sup>17</sup>*CRESST II and X-ray Astrophysics Laboratory, NASA/GSFC, Greenbelt, MD 20771, USA*

<sup>18</sup>*Department of Physics, University of Maryland, Baltimore County, 1000 Hilltop Circle, Baltimore, MD 21250, USA*

### ABSTRACT

We present a detailed compilation and analysis of the X-ray phase space of low- to intermediate-redshift ( $0 \leq z \leq 1$ ) transients that consolidates observed light curves (and theory where necessary) for a large variety of classes of transient/variable phenomena in the 0.3–10 keV energy band. We include gamma-ray burst afterglows, supernovae, supernova shock breakouts and shocks interacting with the environment, tidal disruption events and active galactic nuclei, fast blue optical transients, cataclysmic variables, magnetar flares/outbursts and fast radio bursts, cool stellar flares, X-ray binary outbursts, and ultraluminous X-ray sources. Our overarching goal is to offer a comprehensive resource for the examination of these ephemeral events, extending the X-ray duration-luminosity phase space (DLPS) to show luminosity evolution. We use existing observations (both targeted and serendipitous) to characterize the behavior of various transient/variable populations. Contextualizing transient signals in the larger DLPS serves two primary purposes: to identify areas of interest (i.e., regions in the parameter space where one would expect detections, but in which observations have historically been lacking) and to provide initial qualitative guidance in classifying newly discovered transient signals. We find that while the most luminous (largely extragalactic) and least luminous (largely Galactic) part of the phase space is well-populated at  $t > 0.1$  days, intermediate luminosity phenomena ( $L_x = 10^{34} - 10^{42}$  erg s<sup>-1</sup>) represent a gap in the phase space. We thus identify  $L_x = 10^{34} - 10^{42}$  erg s<sup>-1</sup> and  $t = 10^{-4} - 0.1$  days as a key discovery phase space in transient X-ray astronomy.

*Keywords:* X-ray astronomy (1810), X-ray telescopes (1825), X-ray transient sources (1852), High energy astrophysics (739), Transient sources (1851), Time domain astronomy (2109)

## 1. INTRODUCTION

Transient and variable electromagnetic emission is often associated with the most violent events in space, like stellar explosions, stellar disruptions by supermassive black holes, or accretion-related phenomena on compact objects to name a few. Studying the timescales and intrinsic energy released by each of these phenomena often provide guidance to understand the physics that regulates the bright displays of these transients and variables. To this end, the duration-luminosity phase space (DLPS), where duration is defined as the time between the identification of an outburst and its later non-detection, has been used as a means of placing classes of transient and variable phenomena in the context of their underlying physics and constraining their outburst mechanisms.

Previous works have focused on building an observationally motivated, light curve-populated DLPS for specific wavelength regimes (e.g., Kulkarni 2012; Pietka et al. 2015; Villar et al. 2017 for optical wavelengths, Eftekhari et al. 2022 for millimeter wavelengths, or Metzger et al. 2015 for radio wavelengths), which is facilitated by the significant volume of available data. We build on the first attempts to produce an observation-driven DLPS in the X-rays (Soderberg et al. 2009; O’Brien & Smartt 2013) by populating the DLPS with light curves as a comprehensive view of the low- to intermediate-redshift ( $z \leq 1$ , in order to ensure the sample of sources in the DLPS is representative of the overall demographics presented and that the intrinsic rate of such events is well understood) phase space for (observer frame) 0.3-10 keV transient and variable X-ray phenomena. This extends the use of the DLPS by showing both luminosity and time evolution of these events. The motivation behind compiling this dataset is two-pronged: to identify pristine regions of this parameter space that can be explored by future observing facilities (i.e., identification of discovery areas) and conversely, we can use the phase space location of an unknown type of transient to constrain its intrinsic nature. This dual motivation, both for characterizing the nature of observed events and for identifying discovery frontiers for the future generation of X-ray observatories, makes examination of the phase space vital.

With a number of large scale, all-sky transient surveys that have been carried out at the time of writing (e.g., SRG/eROSITA; Predehl et al. 2021) or are beginning in the immediate future, the DLPS can offer an initial rapid

designation for observed events in tandem with targeted follow-up or before follow-up is initiated. The DLPS is also a resource for retroactive classification of transients recovered from archival data, when follow-up is potentially no longer possible, making it a valuable tool to determine object class from existing observations.

We utilize complete X-ray light curves for a variety of Galactic and extragalactic transient and variable phenomena: gamma-ray burst afterglows, supernovae, supernova shock breakouts and shocks interacting with the environment, tidal disruption events and active galactic nuclei, fast blue optical transients, cataclysmic variables, magnetar flares/outbursts and fast radio bursts, cool stellar flares, X-ray binary outbursts, and ultraluminous X-ray sources. For some classes the data are sparse, and we will instead plot peak X-ray luminosity ( $L_x$ ) vs. duration. In the one case where there were insufficient (*confirmed*) observations, we used theory as a supplement.

We present in Section 2 the datasets for each of the different classes of transient and variable events, and we discuss their location within the DLPS. In Section 3, we examine the use cases for our comprehensive DLPS. Where available, redshifts were used to correct the duration to the rest frame as well as to determine the luminosity distance, assuming a cosmology with  $H_0 = 69.6$  km s<sup>-1</sup> Mpc<sup>-1</sup>,  $\Omega_M = 0.286$ , and  $\Omega_\Lambda = 0.714$ .

## 2. DATA

We assembled X-ray data from a variety of sources. For ease and readability, we include lists of events, as well as their classifications, coordinates, distances, and the relevant literature in Appendix A. Light curve data used in this paper are available on GitHub<sup>1</sup>. In Sections 2.1-2.9, we briefly define each (sub)class of transient/variable, describe their characteristic timescale and luminosity as inferred from their position in the DLPS, and detail the provenance of the light curve data used in this work (summarized in Table 1).

For transient classes – i.e., events that cannot repeat in the same astrophysical object – the light curves are from pointed observations acquired after the detection/identification of the transient. As a result, only a subset of the observations capture the peak X-ray lumi-

<sup>1</sup> <https://github.com/avapolzin/X-rayLCs>; we also include some plotting and preliminary light curve classification helper scripts in this repository.

osity. The situation is somewhat different for variable light curves, some of which include data taken while monitoring the source. We expect that only a fraction of these light curves come from serendipitous detections due to the small field-of-view of the available X-ray instruments.

These data are used in the observational DLPS (Figure 1), where they show the luminosity evolution of observed light curves with time. These same data are used to calculate important X-ray quantities like peak  $L_x$  and isotropic equivalent energy, shown in Figure 2, where clustering by class remains apparent. These summary properties provide a means to characterize the light curves regardless of which stage of outburst they cover.

### 2.1. Gamma-ray Burst (GRB) Afterglows

Gamma-ray bursts (GRBs, Table A1) are burst of  $\gamma$ -rays associated with either the collapse of a massive star (GRBs with a duration of the  $\gamma$ -ray emission  $T_{90} > 2$  s) or the merger of compact objects (i.e. neutron stars and black holes). All GRB X-ray afterglow data shown in Figure 3 were collected via the UK *Swift* Science Data Centre<sup>2</sup> (Evans et al. 2007, 2009), with the notable exceptions of the pre-*Swift* era subluminescent GRBs, GRB980425A (Pian et al. 2000; Kouveliotou et al. 2004) and GRB031203A (Sazonov et al. 2004; Watson et al. 2004). We include long GRBs (lGRBs), short GRBs (sGRBs), ultralong GRBs, and subluminescent GRBs for  $z \leq 1$  in our plotted population where redshift information is available<sup>3</sup>. We also include the X-ray afterglow counterpart of the neutron-star merger event GW170817, for which gravitational-wave emission was detected (e.g., Abbott et al. 2017; Hajela et al. 2019, 2020; Nakar 2020; Margutti & Chornock 2021). We excluded GRBs without well-constrained redshifts as we are interested in luminosity vs. intrinsic duration (rather than fluence vs. observed duration).

Our sample is complete for subluminescent and ultralong GRBs. We include all but one of the long GRBs within  $z = 1$  with X-ray observations from the end of December 2014 through 2019, and all but one of the X-ray observations of short GRBs within  $z = 1$  from 2005 through 2017.

Differentiation of the subclasses of GRBs was informed by the  $T_{90}$  parameter (i.e. the time interval over which 90% of the  $\gamma$ -ray emission is observed). Short GRBs typically have  $T_{90} < 2$  s, long GRBs fall within the  $2 - 10^3$  s range (Kouveliotou et al. 1993), and ultra-

long GRBs have  $T_{90}$  between  $10^3 - 10^4$  s (Levan et al. 2014). We note that some subluminescent GRBs, while having a duration similar to that of long or ultralong GRBs, might actually represent physically distinct phenomena (e.g. supernova shock breakouts see Section 2.2) with  $L_x \lesssim 10^{47}$  erg s<sup>-1</sup> (Norris 2003).

### 2.2. Explosion Shock Breakouts

Shock breakouts (SBOs, Table A2) are the emergence of the first (observable) photons from a stellar explosion. A SBO occurs as the shock goes through the star and reaches an optical depth of  $\tau \sim c/v_{\text{shock}}$  within the star or at the stellar surface or in the stellar wind. Short-duration energetic emission is observable in the X-rays if the shock breaks out from a compact progenitor (Nakar & Sari 2010). SBOs are short duration when their emission peaks in the X-rays, and there is only one broadly accepted observation (Soderberg et al. 2008, see however Mazzali et al. 2008 for a different interpretation), which was a serendipitous detection from a normal type Ib supernova, SN 2008D. While searches of archival data yield potential SBO candidates (e.g. Alp & Larsson 2020; Novara et al. 2020), wide-field X-ray instruments are vital for growing the sample of SBO observations. We note that later analysis of the prompt X-ray signal at the location of SN 2008D showed what is thought to be a breakout from the stellar wind (Balberg & Loeb 2011; Svirski & Nakar 2014). We tentatively include subluminescent GRBs as candidate stellar surface breakouts associated with energetic type Ic-BL supernovae in Figure 3. Subluminescent GRBs are considered candidate stellar surface breakouts by Nakar & Sari (2012), and this possibility is also addressed by Campana et al. (2006), Nakar (2015), and Irwin et al. (2021).

EXMM 023135.0-603743 (Alp & Larsson 2020; Novara et al. 2020), on the other hand, is not included as a candidate in the DLPS due to the uncertain nature of its progenitor. In addition to the possibility that it is a shock breakout from a core-collapse supernova, both Alp & Larsson (2020) and Novara et al. (2020) discuss alternative physical scenarios that could give rise to the observed X-ray transient.

In order to better populate the X-ray phase space (Figure 3), we supplement the proposed stellar surface SBO light curves (from subluminescent GRBs) with results from theoretical calculations by Nakar & Sari (2012). These authors show that:

$$E_{bo} \approx 6 \times 10^{46} E_{53}^{2.3} M_{ej,5}^{-1.65} R_5^{0.7} \text{ erg} \quad (1)$$

$$T_{bo} \approx 700 E_{53}^{1.7} M_{ej,5}^{-1.2} R_5^{-0.95} \text{ keV} \quad (2)$$

$$t_{bo}^{obs} \approx 0.06 E_{53}^{-3.4} M_{ej,5}^{2.5} R_5^{2.9} \text{ s} \quad (3)$$

<sup>2</sup> <https://www.swift.ac.uk>

<sup>3</sup> <http://www.mpe.mpg.de/~jcg/grbgen.html>

**Table 1.** Summary of the classes and subclasses (if any) of transients included in this work.

Class, $N$	Subclass, $N$	Observatories
Gamma-ray Bursts (GRBs), 52		<i>Swift</i> , <i>BeppoSAX</i> , <i>Chandra</i> , <i>XMM-Newton</i>
	Short GRBs (sGRBs), 19	<i>Swift</i> , <i>Chandra</i>
	Long GRBs (lGRBs), 25	<i>Swift</i>
	Ultralong GRBs, 2	<i>Swift</i>
	Subluminous GRBs, 6	<i>Swift</i> , <i>BeppoSAX</i> , <i>Chandra</i> , <i>XMM-Newton</i>
	Wind SBO, 1	<i>Swift</i>
	(Stellar Surface SBOs, 6)	( <i>Swift</i> , <i>BeppoSAX</i> , <i>Chandra</i> , <i>XMM-Newton</i> )
	Type I Core-Collapse, 9	<i>Swift</i> , <i>BeppoSAX</i> , <i>Chandra</i> , <i>XMM-Newton</i> , <i>ASCA</i> , <i>ROSAT</i>
	Type II Core-Collapse, 13	<i>Swift</i> , <i>Chandra</i> , <i>XMM-Newton</i> , <i>ASCA</i>
	Interacting SNe, 9	<i>Swift</i> , <i>Chandra</i> , <i>XMM-Newton</i> , <i>ASCA</i> , <i>ROSAT</i>
	Superluminous SNe (SLSNe), 2	<i>Swift</i> , <i>Chandra</i>
	Ca-rich SNe, 2	<i>Swift</i> , <i>Chandra</i>
	Thermal TDEs, 16	<i>Swift</i> , <i>Chandra</i> , <i>XMM-Newton</i> , <i>ROSAT</i>
	Non-thermal TDEs, 3	<i>Swift</i> , <i>Chandra</i> , <i>XMM-Newton</i> , <i>ROSAT</i>
Tidal Disruption Events (TDEs), 19		<i>Chandra</i> , <i>XMM-Newton</i>
Active Galactic Nuclei (AGN), 8		<i>Swift</i> , <i>Chandra</i> , <i>XMM-Newton</i> , <i>eROSITA</i>
Fast Blue Optical Transients (FBOTs), 5		<i>Swift</i> , <i>BeppoSAX</i> , <i>XMM-Newton</i> , <i>ASCA</i> , <i>ROSAT</i> , <i>RXTE</i>
Cataclysmic Variables (CVs), 41		<i>Swift</i> , <i>Chandra</i> , <i>XMM-Newton</i> , <i>ROSAT</i>
	Novae, 38	<i>Chandra</i> , <i>XMM-Newton</i>
	Dwarf Novae, 3	<i>Swift</i> , <i>RXTE</i>
Magnetar Flares/Outbursts, 15		<i>Swift</i> , <i>BeppoSAX</i> , <i>Chandra</i> , <i>XMM-Newton</i> , <i>ASCA</i> , <i>ROSAT</i> , <i>RXTE</i> , <i>MAXI</i>
	Outburst, 14	<i>Swift</i> , <i>BeppoSAX</i> , <i>Chandra</i> , <i>XMM-Newton</i> , <i>ASCA</i> , <i>ROSAT</i> , <i>RXTE</i>
	Intermediate Flare/Short Burst, 1	<i>Swift</i> , <i>MAXI</i>
Fast Radio Bursts (FRBs), 1		<i>Insight-HXMT</i>
Cool Stellar Flares, 18		<i>XMM-Newton</i>
X-ray Binary Outbursts (XRBs), 17		<i>Swift</i> , <i>Chandra</i> , <i>XMM-Newton</i> , <i>RXTE</i> , <i>eROSITA</i> , <i>NICER</i>
	Low Mass XRBs (LMXRBs), 4	<i>Swift</i> , <i>Chandra</i> , <i>XMM-Newton</i> , <i>RXTE</i>
	High Mass XRBs (HMXRBs), 13	<i>Swift</i> , <i>XMM-Newton</i> , <i>eROSITA</i> , <i>NICER</i>
Ultraluminous X-ray Sources (ULXs), 4		<i>Swift</i> , <i>Chandra</i> , <i>XMM-Newton</i> , <i>ROSAT</i>

NOTE— $N$  indicates the number of included objects. We also list the observatories that were used in the creation of the light curves (including upper-limits). Observatories used include: *Swift* (Burrows et al. 2005), *BeppoSAX* (Boella et al. 1997), *Chandra* (Weisskopf et al. 2000), the X-ray Multi-Mirror Mission (*XMM-Newton*; Jansen et al. 2001), the Advanced Satellite for Cosmology and Astrophysics (*ASCA*; Tanaka et al. 1994), the Roentgen Satellite (*ROSAT*; Trümper 1990), the Spectrum Roentgen Gamma (SRG) extended Roentgen Survey with an Imaging Telescope Array (*eROSITA*; Predehl et al. 2021), the Rossi X-ray Timing Explorer (*RXTE*; Jahoda et al. 1996), the Monitor of All-Sky X-ray Image (*MAXI*; Matsuoka et al. 2009), the Hard X-ray Modulation Telescope (*Insight-HXMT*; Zhang et al. 2020), and the Neutron Star Interior Composition Explorer (*NICER*; Arzoumanian et al. 2014).

<sup>a</sup>We represent the six *candidate* stellar surface shock breakouts, which overlap entirely with the population of subluminal GRBs, in parentheses for completeness.

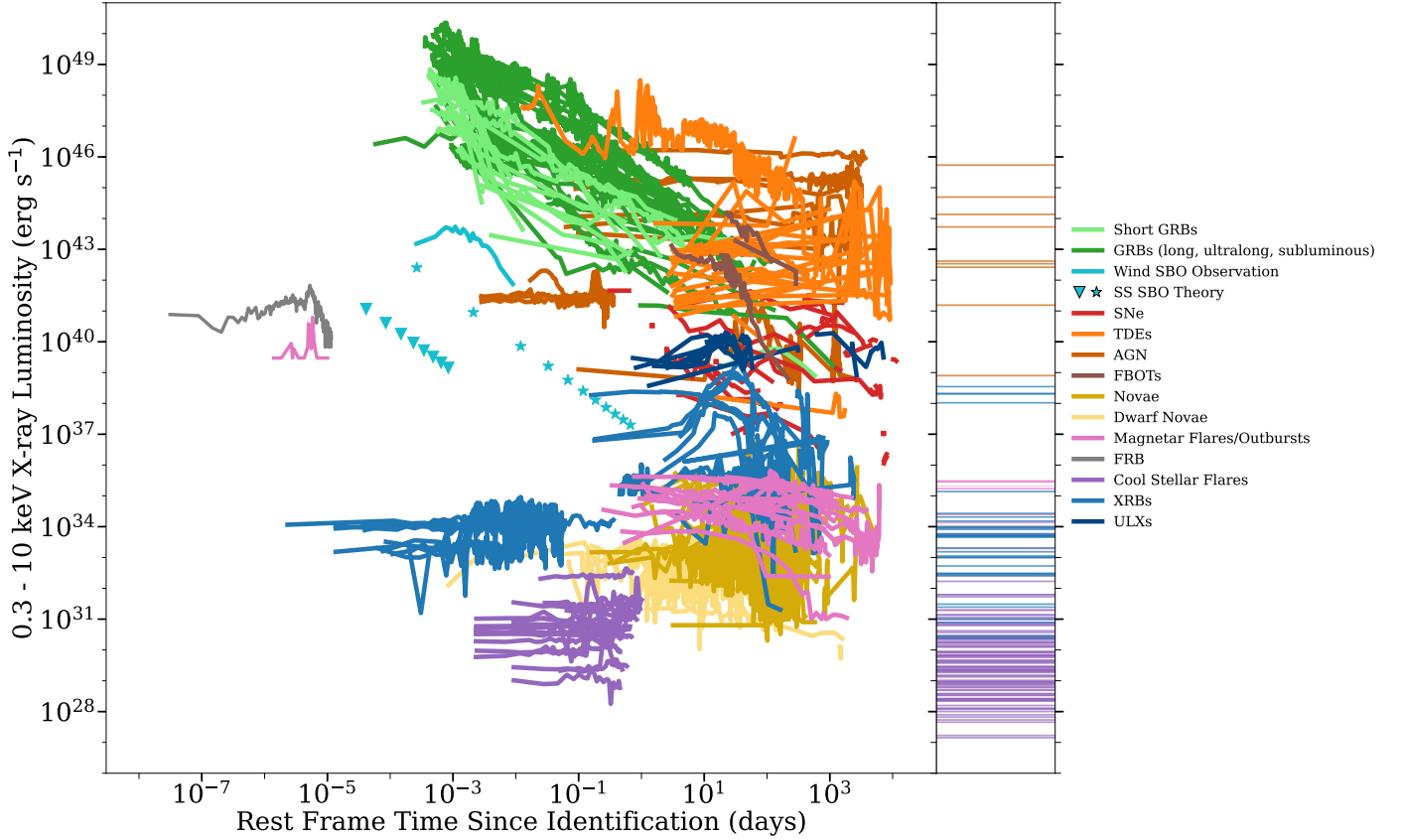


**Figure 1.** X-ray phase space of transients and variable phenomena, including gamma-ray burst (GRB) afterglows, supernovae (SNe), supernova shock breakouts (SBOs), tidal disruption events (TDEs) and active galactic nuclei (AGN), fast blue optical transients (FBOTs), cataclysmic variables, magnetar flares/outbursts and fast radio bursts, cool stellar flares, X-ray binary outbursts, and ultraluminous X-ray sources. *Main Panel:* X-ray luminosity evolution with rest-frame time since identification. Theoretical SBO peak  $L_x$ -duration points are shown with different symbols corresponding to the model's input parameters; see Section 2.2 for details. *Right Side Panel:* To offer a sense of their persistent behavior, the quiescent/pre-flare luminosities of the included variable classes (AGN, magnetar flares/outbursts, cool stellar flares, X-ray binaries, and ultraluminous X-ray sources) are shown as horizontal bars.

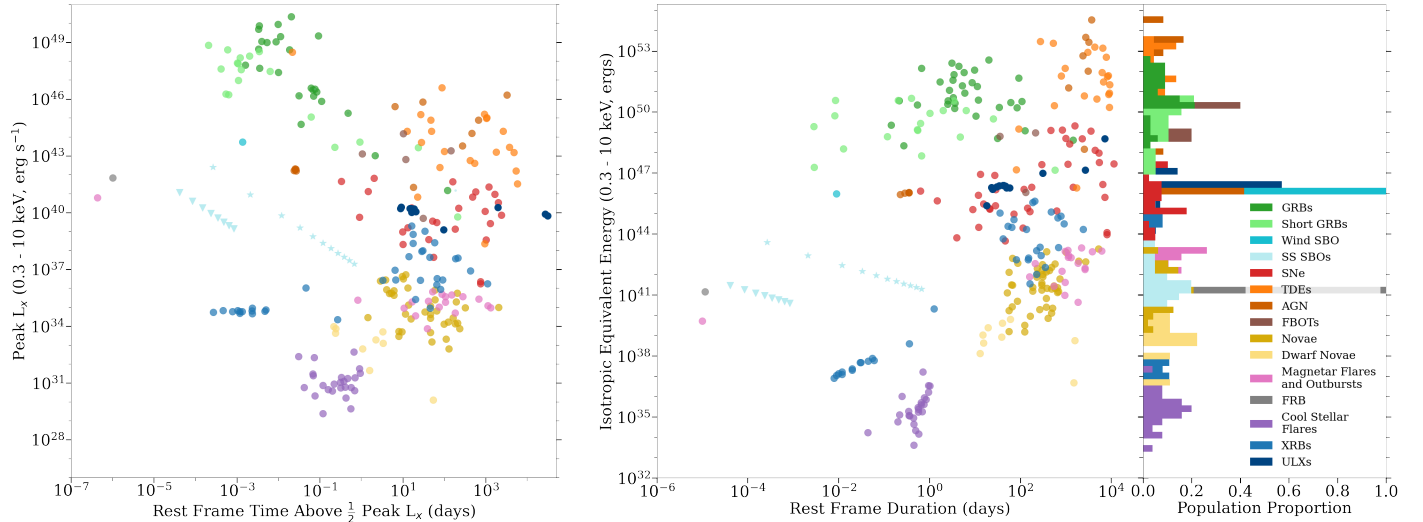


**Figure 2.** *Left Panel:* The peak X-ray luminosity vs. time above half-maximum light. *Right Panel:* At left, the overall energy released during the event vs. the duration of the transient event, and at right, the distribution of isotropic equivalent energies released for each class of transient/variable. As in Figure 1, theoretical SBO peak  $L_x$ -duration point markers correspond to different input parameters in the model. Points are colored according to the class of transient to which they belong; we use the same color coding as in Figure 1 and the histogram at the far right.

$$L_{bo} \approx 4 \times 10^{47} E_{53}^{5.1} M_{ej,5}^{-3.65} R_5^{-1.85} \text{ erg s}^{-1} \quad (4)$$

Where  $E_{bo}$ ,  $T_{bo}$ ,  $t_{bo}^{obs}$ , and  $L_{bo}$  refer to the breakout energy, temperature, observed time (duration), and luminosity respectively.  $E_{53}$  is energy in terms of  $10^{53}$  erg,  $M_{ej,5}$  is the ejecta mass in terms of  $5M_\odot$ , and  $R_5$  is the stellar radius in terms of  $5R_\odot$ .

We use a grid of energy values (between  $10^{51}$  and  $10^{52}$  erg), ejecta mass (between 1 and  $10M_\odot$ ), and stellar radius ( $10^{10}$  and  $10^{11}$  cm, which span the properties of Wolf-Rayet-like stars) to compute  $E_{bo}$ ,  $T_{bo}$ ,  $t_{bo}$ , and  $L_{bo}$  from Equations 1 - 4. Though a red supergiant with a breakout energy of  $10^{52}$  erg is a less likely physical scenario, we include it anyway to account for the full range of possible progenitors that give rise to SBOs within the phase space. Similarly, in order to populate the phase space with potential durations vs. peak luminosities, we limit our plotted sample to those with temperatures (from Equation 2) in the range 0.1-20 keV as representative of the SBOs that will have some X-ray luminosity component in the 0.3-10 keV range of interest. In the upper-right panel of Figure 3, each individual point represents the peak luminosity and duration of a single theoretical stellar surface SBO event.

Shock breakouts from the stellar wind like in SN2008D evolve on timescales ranging from seconds to minutes with  $L_x \sim 10^{42} - 10^{44}$  erg s $^{-1}$ , making it challenging to observe them without wide field of view X-ray instruments facilitating serendipitous detection. Candidate stellar surface SBOs (as potentially in subluminal GRBs) range in luminosity from  $\sim 10^{41} - 10^{47}$  erg s $^{-1}$ , varying on timescales of  $\sim 10^{-4} - 10^{-1}$  days. Our mod-

eled stellar surface SBOs (Nakar & Sari 2012) are somewhat less luminous and shorter-lived, with  $L_x \sim$  a few  $\times 10^{36} - 10^{43}$  erg s $^{-1}$  and  $t \sim$  several  $\times 10^{-5}$  days to  $\sim 1$  day.

### 2.3. Supernovae

Supernova (SN, Table A3) shocks that propagate in the explosion's environment are well-known particle accelerators and well-known sources of X-ray emission as the shocks decelerate and the particles cool down (e.g., Chevalier & Fransson 2017 for a recent review). We collected X-ray data for supernovae from a variety of sources (see Appendix A for details). Because of the rather limited sample of existing observations, we include all available ( $z \leq 1$ ) X-ray light curves in bands with lower energy limits between 0.2 and 0.5 keV and upper energy limits between 8 and 12 keV, which are then k-corrected to the observed 0.3-10 keV energy band assuming a spectrum  $F_\nu \propto \nu^{-\beta}$  with a spectral index  $\beta = 1$  (equivalent to a photon index  $\Gamma = 2$ ), which is consistent with observed spectral properties of SNe in the X-rays (e.g., Li & Pun 2011). Even at the most extreme ends of our allowed input energy limits, using  $\Gamma = 1$  or  $\Gamma = 3$  instead represents a difference of less than a factor of two in luminosity. These k-corrected data are shown in Figure 3.

We divide the SNe into three subclasses based on their underlying physical properties: *Type I core-collapse* to be comprised of Type Ib, Ic, Ib/c, Ic/pec, and Iib SNe; *Type II core-collapse* to be comprised of Type II, IIP, IIL, and Ipec SNe; and *Interacting SNe* (i.e. SNe with

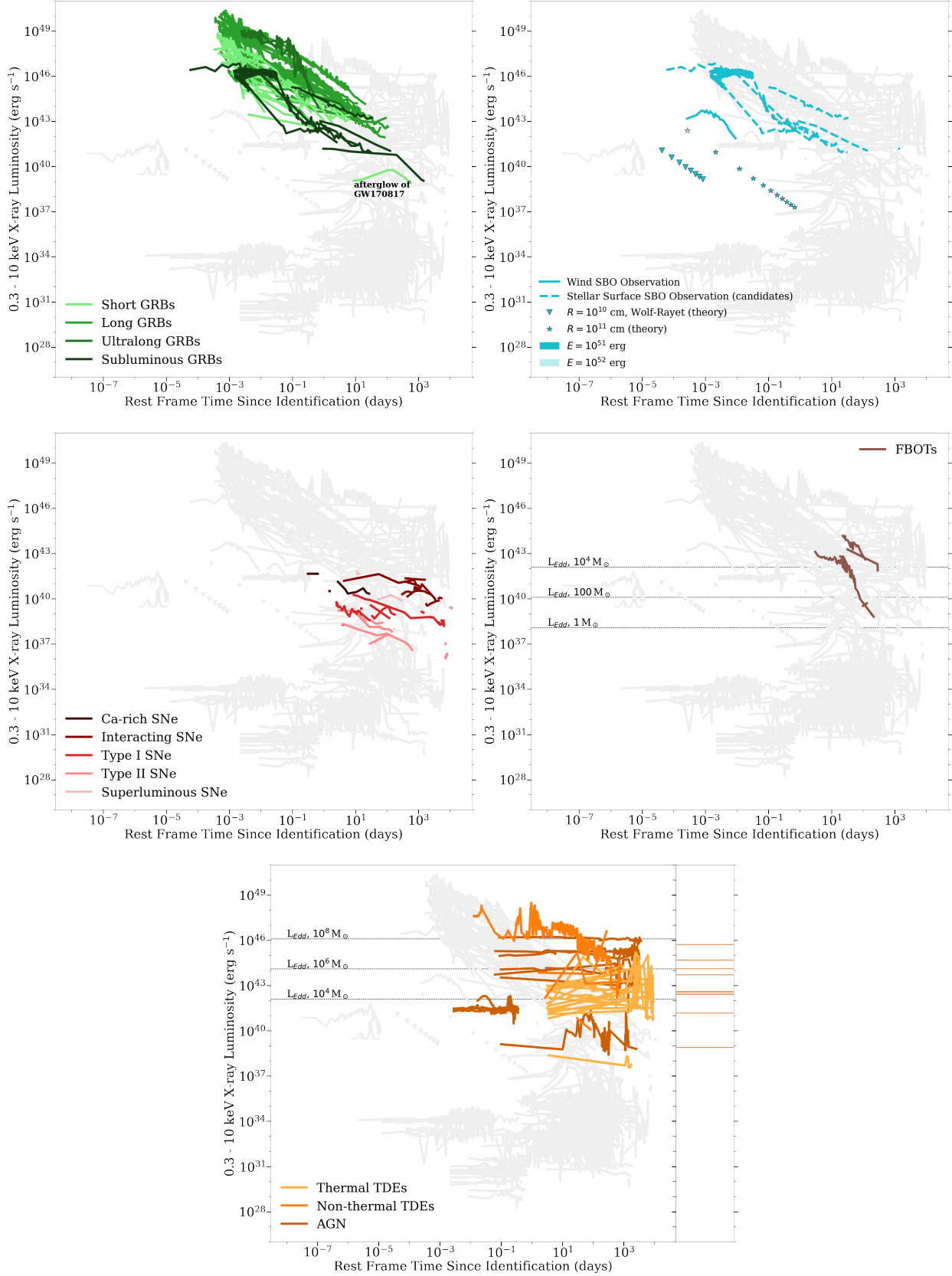


**Figure 3.** X-ray phase space of extragalactic transients, including GRBs, SBOs, SNe, TDEs, AGN, and FBOTs, with all other classes of transient from this work underplotted in gray. Peak luminosity vs. duration are shown as points for modeled SBOs (Nakar & Sari 2012) with input progenitor radius and breakout energy indicated in the legend by  $R$  and  $E$  respectively. We underplot Eddington luminosities (as horizontal dashed lines) for some potentially relevant BH progenitor masses for both FBOTs and TDEs/AGN (Ramsden et al. 2022; Yao et al. 2023). The FBOT X-ray counterparts occupy a luminosity range that is intermediate between normal SNe (shades of red) and GRBs (shades of green). At right in the TDE/AGN subplot, we show pre-flare AGN luminosities for all included AGNs. Included events are listed in Tables A1 through A5.

signatures of CSM interaction in their optical spectra) to be comprised of Type IIn, Ibn, and Ia-CSM SNe. Additionally, we designate (optically) *superluminous SNe* (SLSNe) and *Ca-rich SNe* separately as the two subclasses of SNe for which X-ray emission has been most recently found.

Unlike GRBs, SNe are generally not monitored in the X-rays, in part because they are intrinsically much fainter in the X-rays than GRBs. As a result, they have relatively sparse observations. We include what (non-upper limit) detections are available in the DLPS. We are complete with respect to published X-ray light curves of SNe through the end of 2012, and we have tried to be complete for all non-ordinary SNe (Ca-rich, superluminous, Ia-CSM) with X-ray detections by the time of submission.

Within the DLPS, SNe evolve on timescales ranging  $10^{-1} - 10^4$  days. Ca-rich and interacting SNe have luminosities  $\sim 10^{39} - 10^{42}$  erg  $s^{-1}$  with Ca-rich supernovae evolving on timescales between 0.1 and  $\sim$  hundreds of days and interacting SNe evolving on timescales between 1 day and thousands of days. In general, optically superluminous supernovae are less luminous in the soft X-rays with typical  $L_x \sim$  several  $\times 10^{40}$  – several  $\times 10^{41}$  erg  $s^{-1}$ . Type I core-collapse SNe are slightly less luminous with  $L_x \sim 10^{38} - 10^{40}$  erg  $s^{-1}$ , and Type II core-collapse supernovae are the least luminous with most light curves spanning  $L_x \sim$  several  $\times 10^{35} - 10^{39}$  erg  $s^{-1}$ . Further discussion of the differences in the observed X-ray light curves of different classes of SNe can be found in Dwarkadas & Gruszko (2012) (see Bietenholz et al. 2021 for a similar discussion in the radio).

#### 2.4. Tidal Disruption Events and Active Galactic Nuclei

Tidal disruption events (TDEs, Table A4) occur when a star passes close enough to a black hole that stellar material is accreted, resulting in high energy electromagnetic emission from that accretion (Carter & Luminet 1982, 1983).

We include both TDEs with thermal X-ray emission and non-thermal X-ray emission in Figure 3, using Komossa (2015) and Auchettl et al. (2017) to inform our selection of ( $z \leq 1$ ) TDE candidates, showing only *X-ray TDEs* and “*Likely X-ray TDEs*” from the latter. Our sample of tidal disruption events is complete (and robust – for merging multiple catalogs) until 2017.

TDEs with non-thermal X-ray emission (from hereon, non-thermal TDEs) belong to a subset of  $\sim 10\%$  the TDE population that showed evidence for highly collimated ejecta in the form of relativistic jets (Alexander et al. 2020). There is no evidence for collimation of the

thermal X-ray emission which implies that TDEs with thermal X-rays (from hereon, thermal TDEs) are easier to detect. Because there might be similarities between the flare mechanisms of TDEs and active galactic nuclei (AGN) and the distinction between the two classes can be observationally challenging, we opt to show them both in the bottom panel of Figure 3. In the interest of examining only flaring/outbursting behavior, we include long-term variability from AGN, while we exclude changing-look AGN, which exhibit more persistent variability. We convert the sample of light curves (Auchettl et al. 2018) to our 0.3-10 keV energy band, assuming  $\Gamma = 1.8$  (Tozzi et al. 2006). We note that, though we are far from showing *all* AGN light curves in this energy band, we aim to show a representative sample which demonstrates the difficulty in separating TDEs and AGN from light curves alone (for additional AGN/blazar light curves, see e.g., Giommi et al. 2019).

The Quasi-Periodic Eruptions (QPEs) from GSN 069 (Miniutti et al. 2019) occupy a slightly different (similar luminosity, shorter duration) part of the phase space, with  $L_x \sim 10^{41} - 10^{42}$  erg  $s^{-1}$  and  $\sim 10^{-3} - 10^{-1}$  days (AGN have X-ray luminosities between a few  $\times 10^{38}$  and  $\gtrsim 10^{46}$  erg  $s^{-1}$  and vary on timescales of  $10^{-1}$  to  $10^3$  days; here the low luminosity end of the range is set by NGC 4395, see Auchettl et al. 2018). The physical mechanism that drives QPEs is not fully understood, so we include an example for consistency in looking at AGN outbursting activity, though they may be associated with the same mechanism as changing-look AGN.

While the archetypal non-thermal TDE Swift 1644+57 was initially mistaken for a long GRB, Figure 3 shows that TDEs are clearly distinguished from GRBs for their luminous (non-thermal TDEs have luminosities between  $10^{42}$  and  $10^{49}$  erg  $s^{-1}$ , while thermal TDEs are somewhat less luminous with  $L_x \sim 10^{37} - 10^{45}$  erg  $s^{-1}$ ) and persistent X-ray emission lasting hundreds of days.

#### 2.5. Fast Blue Optical Transients

Fast blue optical transients (FBOTs, Table A5) are a new class of transient astronomical event, only recently recognized in observations and the literature (e.g., Drout et al. 2014; Arcavi et al. 2016; Tanaka et al. 2016; Pursiainen et al. 2018; Ho et al. 2021). In the optical bands these transients are characterized by short rise times (evolution on the timescale of days) and can reach high luminosities ( $L \gtrsim 10^{44}$  erg  $s^{-1}$ ). We include the five known (as of October 2022) X-ray instances of this class – CSS161010 (Coppejans et al. 2020), AT2018cow (Rivera Sandoval et al. 2018; Margutti et al. 2019; Rivera Sandoval et al. 2019), AT2020xnd (Bright et al. 2022; Ho et al. 2022), AT2020mrf (Yao et al. 2022), and



AT2022tsd (Schulze et al. 2022; Matthews et al. 2022) – in our phase space plot, Figure 3. Until now, only the most luminous optical FBOTs (collectively referred to as Luminous FBOTs – LFBOTs) have exhibited detectable X-ray counterparts.

### 2.6. Cataclysmic Variables

Cataclysmic variables (CVs, Table A6) are binary systems undergoing mass transfer in which a white dwarf accretes material from a low-mass main sequence companion. The conditions of that mass transfer define the characteristics of the CV outburst. Here we look exclusively at the two classes of CVs that exhibit bursting behavior<sup>4</sup> – (classical and recurrent) novae and dwarf novae.

A classical/recurrent nova outburst occurs when the accreted material causes thermonuclear runaway on the surface of the white dwarf, resulting in highly energetic ejection of material from the stellar surface. All X-ray data of these novae are from Mukai et al. (2008) and Page et al. (2020); we include all classical/recurrent novae detected between 2006 and 2017. In the instances where we have both an upper- and lower-limit luminosity for various novae in Mukai et al. (2008), we utilized both, to return a *lower-* and *upper-*limit light curve, offering us a greater sense of where novae can, and do, exist in the X-ray phase space (Figure 4). Where k-corrections are necessary to shift data into the (observer frame) 0.3-10 keV energy band, we adopt a thermal bremsstrahlung spectral model with  $kT = 5$  keV following Mukai et al. (2008).

The X-ray emission in dwarf novae stems from the inner accretion flow region around the white dwarf. During the outburst, the mass transfer rate through this inner region increases. As a result it is expected that the X-ray emission ( $\geq 2$  keV) will briefly increase, but then be suppressed as the optical depth of this region increases. This behavior can be seen in multi-wavelength light curves of the dwarf nova SS Cygni (e.g., Wheatley et al. 2003; Russell et al. 2016). Note that there are a number of unanswered questions about this model (see Mukai 2017), and no other dwarf novae show this exact behavior (e.g., Fertig et al. 2011; Mukai 2017). As we are interested in the DLPS of systems that show X-ray brightenings, we limit our sample to those dwarf novae that show X-ray brightenings during optical outburst (see Table A6). The three dwarf novae included here are those with good temporal coverage and multi-

wavelength data that supports enhancement in the X-rays. There are  $\sim 8$  other DNe that show this same brightening, but each has only  $\sim 1$  detection in outburst.

CV outbursts are fairly low luminosity in the  $L_x \sim 10^{28} - 10^{36}$  erg s<sup>-1</sup> range, with dwarf novae only reaching a peak  $L_x \sim 10^{34}$  erg s<sup>-1</sup> and classical/recurrent novae spanning that entire range. They evolve on timescales ranging from seconds to years.

### 2.7. Magnetar Flares/Outbursts and Fast Radio Bursts

Magnetar flares/outbursts (Table A7), driven by perturbations in the strong magnetic field of the magnetar, come in three broad flavors: giant flares (to date, only observed in the hard X-rays and gamma rays), outbursts (characterized by a decay on the scale of days), and intermediate flares/short bursts (lasting milliseconds to tens of seconds). At gamma-ray energies, the three observed giant flares started with a short (0.1–0.2 s) flash with luminosity from  $\approx 10^{44}$  to  $10^{46}$  erg s<sup>-1</sup>, which was followed by a tail lasting a few hundreds of seconds and modulated at the pulsar spin period. In all three events, the total energy of the tail was  $\approx 10^{44}$  erg (e.g. Esposito et al. 2021). While it is likely that a comparable amount of energy was emitted in the soft X-ray band (see Rea et al. 2013), we lack reliable measurements of their properties in that band.

Though intermediate flares and short bursts are often referred to separately, Israel et al. (2008) suggest that these events actually occur along a continuum of spectral properties (though not a continuum in duration or fluence). Making an arbitrary cut, where intermediate flares persist longer and are brighter while short bursts are lower energy and shorter duration, is not based on intrinsically different physics. For the purposes of simplicity in our sub-classifications, we consider intermediate flares and short bursts to be a single population, characterized by  $L_x \sim 10^{39} - 10^{41}$  erg s<sup>-1</sup> and varying on extremely short timescales  $\sim 10^{-6} - 10^{-4}$  days.

We used the Magnetar Outburst Online Catalog (Coti Zelati et al. 2018) for most of the *outburst* data ( $L_x \sim 10^{31} - 10^{46}$  erg s<sup>-1</sup> with variation on timescales  $\sim 10^{-1} - 10^4$  days), also including data from Rea et al. (2016) and Esposito et al. (2019) in order to build a *representative* sample. Plotting each light curve from the beginning of the outburst itself, we show each recurrent event from the same progenitor separately.

In order to elucidate the variable nature of these magnetars, we compare their luminosity in outburst (or during a flare) to their quiescent luminosity; we retrieve

<sup>4</sup> We do not include light curves from non-outbursting CVs, like polars, which exhibit low amplitude flickering and flaring due to their stronger magnetic fields (e.g., Angelini & Verbunt 1989).

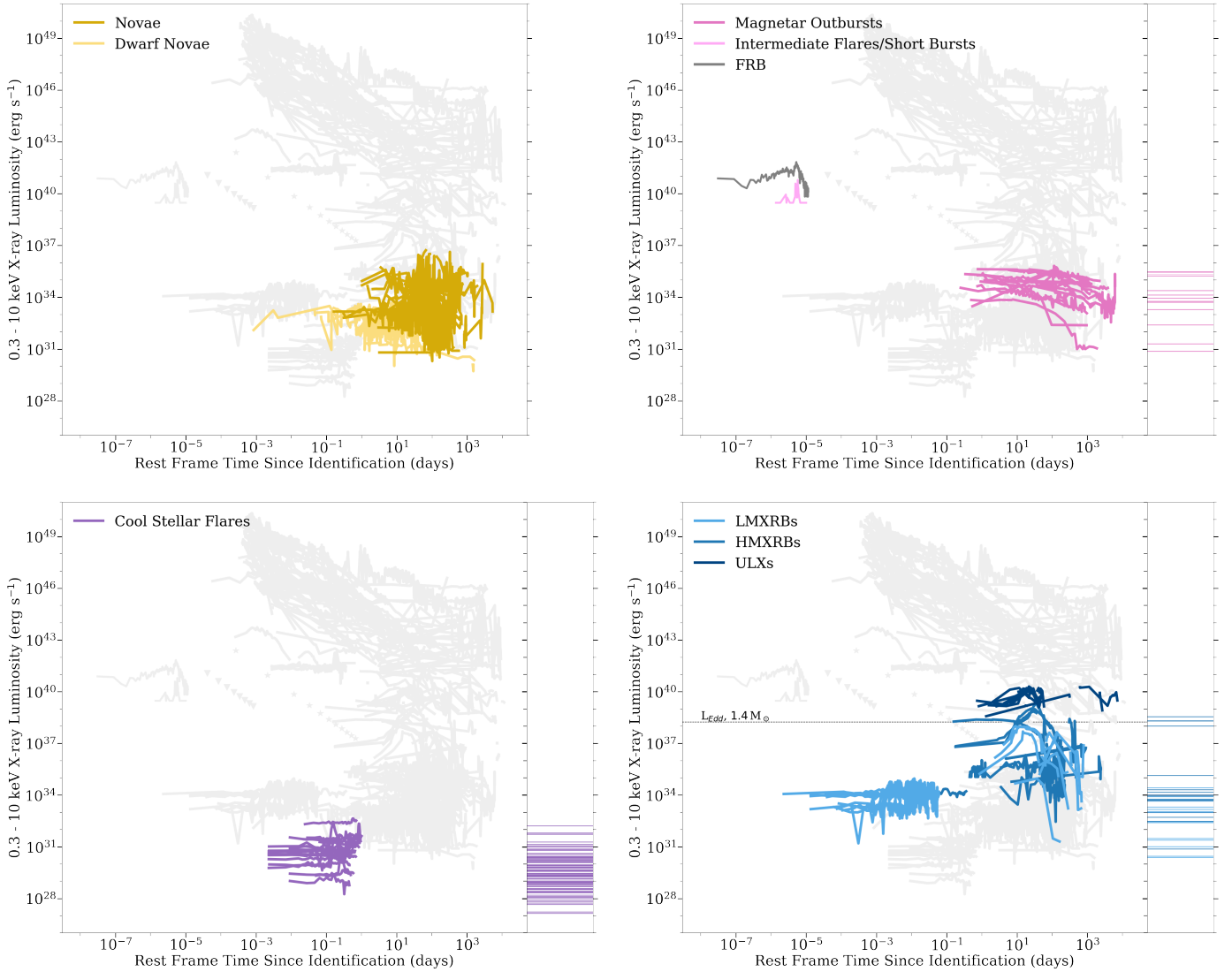


**Figure 4.** X-ray phase space of Galactic (CVs, magnetar flares/outbursts, and cool stellar flares) and Galactic/extragalactic (XRBs, ULXs, and FRBs) transients and variables, including those classes of event with some signals which have been observed to originate within the Galaxy, such as CVs (novae and dwarf novae), magnetar flares and outbursts, fast radio bursts (specifically the Galactic FRB200428), cool stellar flares, XRBs, and ULXs. We underplot the Eddington luminosity for a  $1.4 M_{\odot}$  progenitor for additional context in the XRBs/ULX panel. With the exception of the CV subplot, at right, we show quiescent luminosities for each class of object. Included events are listed in Tables A6 through A9.

these data from Olausen & Kaspi (2014)<sup>5</sup> in the 2-10 keV energy band. We employ a k-correction, to appropriately relate these luminosities to the 0.3-10 keV behavior we have emphasized throughout the X-ray phase space plot, given a power law, black body, or power law + black body model individual to the source from Olausen & Kaspi (2014). Where a spectral fit is not offered, we use a generalized multiple component spectrum ( $\Gamma \sim 2$ ,  $kT_{low} \sim 0.3$  keV,  $kT_{high} \sim 0.6$  keV) in quiescence (Mong & Ng 2018). Further, to ensure a

one-to-one comparison of the emission from quiescent magnetars and those actively exhibiting variable behavior, we restrict our quiescent  $L_x$  sample to match the magnetars shown in the X-ray phase space plot (Figure 4).

Due to the extremely fleeting nature of the short bursts and intermediate flares, much of the data comes from serendipitous triggers, many of which occur in the harder X-rays, since the current class of wide-field instruments operate in the hard X-rays/gamma-rays. This accounts, in part (or in whole), for the paucity of observations for these phenomena in the soft X-rays (and so

<sup>5</sup> <http://www.physics.mcgill.ca/~pulsar/magnetar/main.html>

in our phase space plot) relative to the frequency with which they occur.

Fast Radio Bursts (FRBs) are extremely short duration transient events characterized by an intense burst of radio emission (Lorimer et al. 2007; or see Petroff et al. 2019 and Petroff et al. 2022 for reviews). Multiwavelength follow-up has been conducted to detect counterparts in other wavelength regimes, but efforts have been largely unsuccessful (e.g., Chen et al. 2020). Recently, though, the SGR 1935+2154 outburst on 2020 April 28 has been the subject of discussion as a candidate for an X-ray counterpart to FRB 200428 (The CHIME/FRB Collaboration et al. 2020; Bochenek et al. 2020). Concurrent radio and X-ray emission from this source was detected again in October 2022 (Dong & CHIME/FRB Collaboration 2022; Wang et al. 2022).

Because there is evidence linking this event to a magnetar progenitor, we include the FRB light curve (Li et al. 2021) in Figure 4. The coincident X-ray event from SGR 1935+2154 is consistent with the apparent continuum behavior of magnetar outbursts, flares, and bursts across the phase space (with  $L_x \sim 10^{40} - 10^{42}$  erg  $s^{-1}$  on timescales  $\sim 10^{-8} - 10^{-5}$  days) and is indicative of the possibility that some FRBs might be the radio counterparts to soft gamma repeaters (see however Pleunis et al. 2021).

### 2.8. Cool Stellar Flares

Cool, low mass stars (Table A8), such as M-dwarfs, can be highly variable, with energetic flares driven by magnetic reconnection events. The intensity of this behavior is also correlated with age, with younger low-mass stars exhibiting more variability.

We place data from Pye et al. (2015) in Figure 4 and assume a thermal spectral model with a temperature of  $kT = 1.5$  keV in order to perform the flux conversion. Dwarf stars included in our sample are K, M, and L types. As in Section 2.7, quiescent luminosities (digitized from Pye et al. 2015) are plotted at the right to appropriately contextualize the flares and offer yet more indication of where these flaring stars exist in the X-ray phase space. Cool stellar flares are relatively short duration, with timescales ranging from on the order of hundreds of seconds up to  $\sim 1$  day. They are also low luminosity<sup>6</sup> events with  $L_x \gtrsim 10^{28}$  erg  $s^{-1}$  and up to several  $\times 10^{32}$  erg  $s^{-1}$ . Quiescent luminosities span the range  $\sim 10^{27} - 10^{32}$  erg  $s^{-1}$ .

<sup>6</sup> We note that all sky survey data has shown intrinsically rare flares up to  $L_x \sim 10^{34}$  erg  $s^{-1}$  at slightly higher energies (2 - 20 keV; Tsuboi et al. 2016).

### 2.9. X-ray Binary Outbursts and Ultraluminous X-ray Sources

X-ray binaries (XRBs, Table A9) are stellar binaries where a compact object (neutron star or black hole) is accreting material from its companion, causing energetic outbursts. Ultraluminous X-ray sources (ULXs, characterized by peak  $L_x > 10^{39}$  erg  $s^{-1}$ , independent of the source’s underlying mechanism) are frequently associated with super-Eddington XRBs. We also elect to group them here, showing them in the same subplot of Figure 4. XRBs are further broken out into high mass (HMXRBs, with a companion star of mass  $\gtrsim 10 M_\odot$ ; for a review, see Reig 2011) and low mass (LMXRBs, generally with a  $M \lesssim 1.5 M_\odot$  companion; for a review, see Tetarenko et al. 2016) populations. The former includes BeXRBs, supergiant X-ray binaries (SGXRBs), and supergiant fast X-ray transients (SFXTs), while the latter includes neutron star X-ray binaries (NS-XRBs), black hole X-ray binaries (BH-XRBs), and, though we do not have any in our DLPS sample, very faint X-ray transients (VFXTs; Heinke et al. 2015) or very faint XRBs. Details of the relevant data and their provenance are in Table A9.

As with the other variable signals (magnetar outbursts and cool stellar flares, top right and bottom left of Figure 4), we plot the quiescent  $L_x$  of ULX and XRB events at the right in Figure 4. As in Section 2.7, for the purposes of this paper, we define the quiescent luminosity as the lowest recorded X-ray luminosity, opting for simplicity rather than a more stringent definition that might not designate this persistent, non-outburst behavior as quiescence. Though we are not aiming for completeness, choosing instead to use a *representative* sample, the XRB and ULX coverage of the phase space is clear for relatively long timescales ranging from tenths to thousands of days and intermediate luminosities. XRBs exist in roughly the  $L_x \sim 10^{32} - 10^{39}$  erg  $s^{-1}$  range (with quiescent luminosities between  $10^{30}$  and  $10^{35}$  erg  $s^{-1}$  and outburst  $L_x \gtrsim 10^{35}$  erg  $s^{-1}$ ). ULXs have luminosities greater than several  $\times 10^{38}$  erg  $s^{-1}$  and up to  $\sim 10^{40}$  erg  $s^{-1}$ , with quiescent  $L_x$  falling between  $10^{38}$  and  $10^{39}$  erg  $s^{-1}$ .

In regards to target selection, it is necessary to use a sample of sources with well-measured distances. We note that many of the Galactic HMXRBs have poorly measured distances with high uncertainties (e.g. Bartlett et al. 2019; Ferrigno et al. 2022), while their soft X-ray spectra might suffer from strong absorption. However, nearby galaxies of the Small and Large Magellanic Clouds (i.e. SMC and LMC) have well defined distances, low foreground absorption and an abundance of HMXRBs (Haberl & Sturm 2016). Thus a represen-

tative sample of HMXRB outbursts was obtained from the SMC and LMC.

### 3. DISCUSSION

#### 3.1. *Unclassified X-ray Sources: A Short Case Study*

With the rise of time-domain astronomy, there has been a commensurate increase in opportunities to capture new types of transient/variable events that defy all known classification schemes. In some cases, these events have been discovered in archival data searches, thus preventing real time follow-up of these events outside the X-rays. This has practically prevented the identification of the true underlying nature of these new classes of events. In Figure 5, we plot a selection of these yet-unidentified “oddballs” (Jonker et al. 2013; Glennie et al. 2015; Irwin et al. 2016; Bauer et al. 2017; Xue et al. 2019; Novara et al. 2020) to illustrate how they fit into the larger X-ray phase space. We include only those with known or estimated distances (assuming for the purposes of this case study that the X-ray phase space of transients for  $z \leq 1$  is similar to the phase space of transients at all redshifts), and spectra for those observed outside of the 0.3 - 10 keV energy band to facilitate a k-correction.

Where multiple distance estimates are given, we include light curves at each of those distances to better fill out the *uncategorized* X-ray phase space and demonstrate the potentially varied interpretations of these signals at different redshifts. Though they are sometimes referred to as fast X-ray transients (FXTs or FXRTs, see e.g. Quirola-Vásquez et al. 2022, 2023 for a population-level examination), the light curves point to these transients having a variety of progenitors. This inhomogeneous class of transient events evolves on timescales of  $\sim 10$ s of seconds to days and spans roughly 21 dex in luminosity.

Where the discovery papers have broadly speculated about the origin of these transients, we have colored the “oddball” light curves accordingly, allowing their position in the DLPS to discriminate between equally likely physical scenarios. In fact, this is an extension of the analysis done in Bauer et al. (2017), where they illustrate potential classifications by comparing CDF-S XT1 to light curves from already classified events. Where no one potential class is favored in the discovery paper we choose to leave the light curve *uncategorized* in the X-ray phase space (CDF-S XT1), whereas we color those with a single (or preferred) proposed origin according to that theory (XRT 000519, XRT 120830, and XRT 110103, EXMM 023135.0-603743). Jonker et al. (2013) prefers the (beamed) tidal disruption of a white dwarf by an intermediate mass black hole for XRT 000519, though

our results suggest that an X-ray flash (as would be associated with a GRB) would also be reasonable. Taking XRT 000519 as potentially related to XRT 110103, Glennie et al. (2015) suggest the same potential progenitors for that event. They also indicate that XRT 120830 seems consistent with a dwarf star flare, which is borne out by its position in the phase space. Eapachen et al. (2022) examines the potential host galaxies of XRT 000519 and XRT 110103 in order to place constraints on the nature of the FXTs; though no potential host was detected for XRT 110103, XRT 000519 appears associated in projection with a distant galaxy candidate, seemingly favoring a beamed TDE or a binary neutron star merger like the one responsible for GW170817.

Sources 1 and 2 (Irwin et al. 2016) are ultraluminous X-ray outbursts in NGC 4636 and NGC 5128 respectively. Though their behavior is largely consistent with soft gamma repeaters or anomalous X-ray pulsars (their position in the DLPS matches the anticipated position of intermediate luminosity/duration magnetar flares and outbursts), the stellar populations of their hosts make this scenario unlikely. It is also possible that they are outbursts due to accretion onto neutron stars (though they are super-Eddington in this scenario, these events are somewhat shorter in duration than the other ULXs in the DLPS) or intermediate mass black holes. In the context of the duration-luminosity phase space, Sources 1 and 2 are also consistent with the anticipated position of smaller, lower energy stellar surface shock breakouts. CDF-S XT2 (Xue et al. 2019) has been identified as having emission consistent with a magnetar-driven outburst, potentially from a binary neutron star merger. Its position in the DLPS is strikingly similar to the included population of short gamma-ray bursts. Xue et al. (2019) rule out long gamma-ray bursts and shock breakout-like events due to the luminosity and luminosity evolution and point out that a beamed TDE is also unlikely due to the short timescales on which that evolution occurs. Similarly, Novara et al. (2020) posit that EXMM 023135.0-603743 could be a shock breakout from a core-collapse supernova, a possibility which is supported by the light curve’s position in the phase space, while also noting that it could be an AGN (within the DLPS, EXMM 023135 also overlaps almost entirely with the QPE GSN 069), a TDE, or even a late-time observation of a giant flare from a magnetar, though each of those scenarios is disfavored given other concurrent data (Novara et al. 2020).

Ultimately it is clear that, while the DLPS is not able to provide classification for transients/variables without input from the signal’s spectral evolution and from other investigations that hint at the underlying mechanism, it

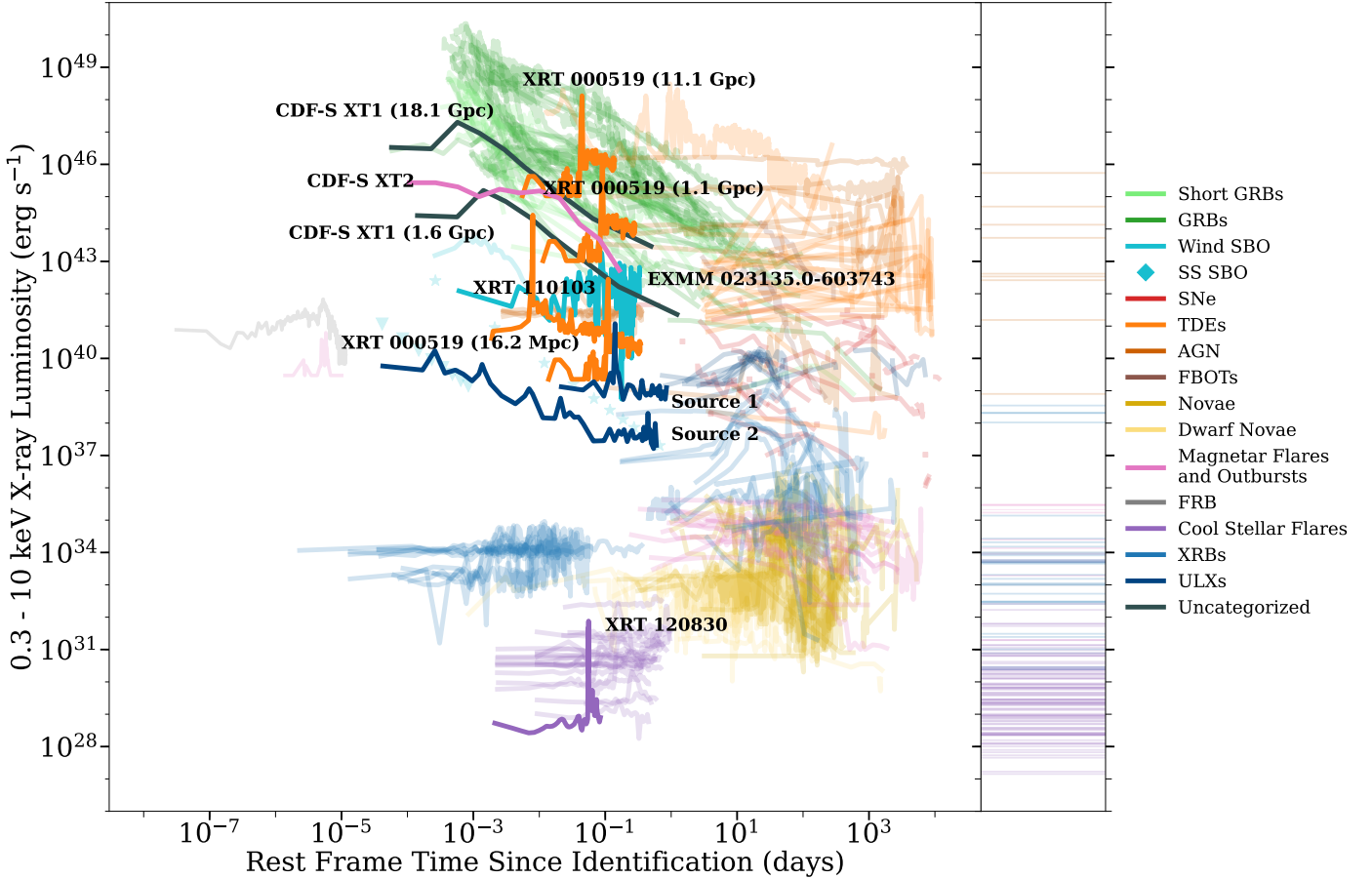


**Figure 5.** We compare existing observations of transients with unclear/debated classification (Table A10) with our established X-ray phase space as described in Section 3.1. These signals are colored according to their preferred classification, though in cases where no one model is considered a better match (CDF-S XT1), we give them their own “oddball” color to differentiate them from the already classified transients in the phase space. For sources with uncertain distance estimates, each estimate is shown, with the relevant distance stated in parentheses. Included events are listed in Table A10.

is extremely useful to contextualize potential and preliminary classifications. As we see looking at the 16.2 Mpc XRT 000519 light curve and XRT 110103, their position in the phase space is apparently more consistent with an AGN/QPE than with a TDE, the potential confusion in classification stemming from the innate difficulty in distinguishing TDEs and AGN. For greater distances, the light curve characteristics of XRT 000519 seem to potentially align with a GRB-related X-ray flare. Similarly, while CDF-S XT1 has a myriad of potential progenitors (among them, an off-axis short GRB or a subluminal GRB, another white dwarf-intermediate mass black hole TDE; Bauer et al. 2017), the light curve (assuming a distance of 18.1 Gpc) is nicely consistent with the subluminal GRBs in our sample.

3.2. Discovery Space

As we enter a new era in the search for/detection of X-ray transients and variables, due to both large time-

domain surveys and next generation X-ray observatories, it is crucial to understand the observational restrictions that have inherently shaped our understanding of the high energy transient sky to now. In examining the phase space of existing detections, we find that while both the most luminous (largely extragalactic) and least luminous (largely Galactic) part of the phase space is well-populated at  $t > 0.1$  days, intermediate luminosity phenomena ( $L_x = 10^{34} - 10^{42}$  erg  $s^{-1}$ ) represent a gap in the phase space. We thus identify  $L_x = 10^{34} - 10^{42}$  erg  $s^{-1}$  and  $t = 10^{-4} - 0.1$  days as a key discovery phase space in transient X-ray astronomy (see Figure 6).

The most obvious constraints are the sensitivity limits of current instruments and the difficulty of rapid response to a fleeting and intrinsically rare signal, which leave gaps in our phase space at low luminosities and short durations respectively. Due to inherent design constraints (see Figure 7, discussed more in Section 3.3) current instruments generally fall into one of two cate-

gies – instruments that are likely to contribute to the serendipitous discovery of soft X-ray transients, which have limited sensitivity and instruments that allow for follow-up of event evolution down to very deep limits, which are extremely limited in their field of view.

Instruments with a wide field of view will serendipitously detect many more events than targeted instruments, contributing to the discovery of transient signals alongside survey instruments. Realistically, extremely short-duration events (on the order of seconds) will not be observed with any regularity without a new generation of wide field instruments. This regime of extremely rapid events is already known to include FRB X-ray counterparts and their likely relatives, magnetar flares.

Target of Opportunity (ToO) protocols and other similar observational triggers play a role in successful follow-up of transitory signals. Greater efficiency in the form of fast re-pointings will also help push toward observation of extremely short-duration events; for instance, the robust *Swift* ToO process is well-established. Automated follow-up is not restricted to the X-ray, with high-energy transient detections triggering radio observations (e.g. Staley et al. 2013; Hancock et al. 2019), as well.

Projects such as Exploring the X-ray Transient and variable Sky (EXTraS; De Luca et al. 2021) aim to address the gap in the short duration phase space at the algorithmic level, extracting previously unidentified signals and variability from existing XMM-Newton data (e.g., Novara et al. 2020). Efforts to rapidly disseminate information about detections like the Living *Swift*-XRT Point Source catalog (Evans et al. 2022) offer yet other opportunities for expedient analysis and follow-up. Similarly, it is possible that mining *unrelated* X-ray observations (for example, those intended to study the hot halos of galaxies) for transients in real time provides another avenue for serendipitous detection.

More sensitive instruments are key for targeted follow-up. The next generation of highly sensitive soft X-ray missions will enable us to track the evolution of light curves to much later times/lower luminosities as they decay and will provide a broader understanding of transient populations, as in many cases, we are currently only meaningfully sampling the most luminous end of the population.

Figure 6 also reveals an under-sampled area of the phase space that we should aim to explore. On the interval  $L_x = 10^{34} - 10^{42}$  erg s<sup>-1</sup> and with timescales between  $10^{-4}$  and  $\sim 0.1$  days, there is a clear gap in the phase space. This gap also corresponds to some known physical phenomena – stellar surface shock breakouts (see Section 2.2) and the continuum behavior between

magnetar flares and outbursts (see Section 2.7). Efforts to expand observations in this regime should be motivated by the probable detection of these missing signals.

### 3.3. Rates of transient discovery

There is a well-known trade-off between instrument FOV and sensitivity, as shown in Figure 7, using specifications from currently operating and proposed missions: larger FOVs tend to correlate with lower sensitivities.

Making the reasonable assumption that we have already observed, and included in our DLPS, the most luminous events from each subclass of transient/variable, we can decouple the advantages of increased FOV and increased sensitivity with transient peak luminosities and volumetric rates from Stone & Metzger (2016), Coppejans et al. (2020), Margutti & Chornock (2021), and Ghirlanda & Salvaterra (2022), separately examining the importance of wide-field instruments and extremely sensitive instruments. For the GRBs (both long and short), we apply a beaming correction factor based on a conservative jet opening angle of  $\sim 3^\circ$  (Fong et al. 2015; Rouco Escorial et al. 2022). Calculating the maximum distance out to which each class of transient can be observed based on instrument sensitivity,  $d_L = \sqrt{L_{\max}/(4\pi \times \text{sensitivity})}$ , we can use a three-dimensional observing volume, defined as  $\frac{\text{FOV}}{\Omega} \times \frac{4}{3}\pi d_{\text{com}}^3$  (where FOV is the instrument field of view,  $\Omega$  is the solid angle of the sky, and  $d_{\text{com}}$  is the maximum comoving distance out to which each class of transients can be observed inferred from  $d_L$  and the cosmology in Section 1), to ascertain the number of anticipated transient observations per year for instruments of varying sensitivity and FOV.

We can isolate the impact of increased FOV by effectively marginalizing over sensitivity and looking at the number of observations as a function of field of view. We choose a representative sensitivity of  $10^{-13}$  erg s<sup>-1</sup> cm<sup>-2</sup>, corresponding to the median flux limit of the instruments listed in Table 2, and assume a static pointing, so that the importance of signals serendipitously falling in that FOV is clear. We show this plot on the left side of Figure 8. Similarly, we can look at the importance of increased sensitivity by selecting a representative FOV (1 deg<sup>2</sup>, corresponding to the median FOV among instruments in Table 2) and plotting the number of detections per class of transient as a function of sensitivity. This is shown on the right side of Figure 8. As in the rest of the paper, we limit our events and observing depths to the redshift range in which their rates are well-constrained ( $z \leq 1$ ). It is then apparent that, for detection of bright sources like GRBs, TDEs, SBOs, and FBOTs within  $z = 1$ , there is little, if anything, to be gained by im-

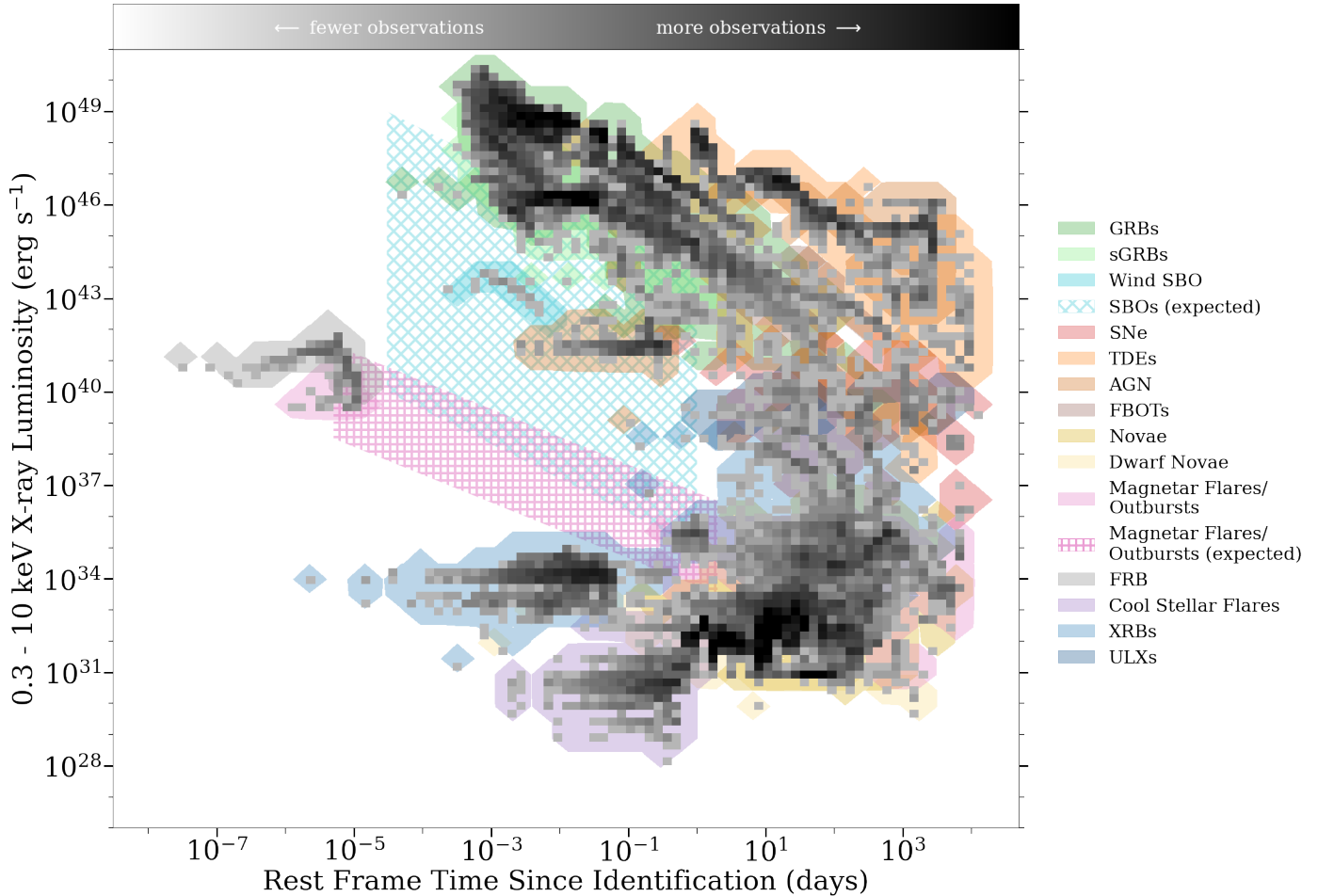


**Figure 6.** The density of light curves in our phase space with the corresponding classes of transient underplotted; the colorbar is logarithmic and larger bins were used for the transient classes than for the overall observations. Though we only show the density of the representative data included in this paper (and so not the comprehensive density of *all* observations in this energy band, though this sample should span a representative range in observed X-ray luminosity and duration), certain trends are notable that are generally relevant, including that the best sampled classes of transient are either Galactic phenomena (such as cool stellar flares or novae) or high luminosity extragalactic transients such as GRBs and short GRBs and that there is a paucity of observations of relatively short duration events at intermediate luminosities. We use hatches to mark the general region of the phase space where we would anticipate, but do not yet have, observations of magnetar flares and outbursts (pink) and shock breakouts from stellar explosions (light blue) among other events. We note that, though it is possible that the soft X-ray emission from giant flares of magnetars may be comparable in luminosity to what has been observed in the hard X-rays (peak  $L_x \sim 10^{47}$  erg s $^{-1}$ ; Hurley et al. 2005), given the paucity of soft X-ray observations of giant flares, we define the “expected” region of the DLPS for magnetar flares and outbursts based on available data.

proving instrument sensitivity beyond a 1 ks flux limit  $\sim 10^{-14}$  erg s $^{-1}$  cm $^{-2}$ ; instead, wide FOV instruments will be critical to the discovery and observation of these events.

We can also use each class’s maximum luminosity along with the instrument sensitivity to determine the distance out to which each transient/variable event can be observed. We take the maximum luminosity of the transient in the GRB, SBO, SN, TDE, CV, magnetar flare/outburst, cool stellar flare, XRB, ULX, FBOT, and FRB categories to represent the most luminous end of their respective distributions. We then apply the 0.3-10

keV flux limit (as in Figure 7 and Table 2) to determine the luminosity distance out to which the transient can be detected, from which we estimate the comoving distance.

For Galactic transients (i.e., CVs, magnetar flares/outbursts, and cool stellar flares) and Galactic/extragalactic transients (i.e., XRBs, ULXs, and

**Table 2.** Soft X-ray imaging instrument performance parameters.

Instrument	Energy band (keV)	Flux limit <sup>a</sup> (erg s <sup>-1</sup> cm <sup>-2</sup> )	FOV	References
ROSAT/PSPC-C	0.1 - 2.5	$\sim 10^{-13}$	3 deg <sup>2</sup>	Trümper 1990; Briel et al. 1996 Greiner et al. 1999
Chandra ACIS-S <sup>b</sup>	0.5 - 7	$\sim 3 \times 10^{-14}$	16'9 × 16'9	Chandra X-ray Center et al. 2021
Swift/XRT	0.3 - 10	$\sim 2 \times 10^{-13}$	23'6 × 23'6	Burrows et al. 2005 Evans et al. 2020
MAXI GSC	2 - 30	$\sim 9 \times 10^{-11}$	160° × 3°	Sugizaki 2010
MAXI SSC	0.5 - 12	$\sim 2 \times 10^{-10}$	90° × 1'5	Tsunemi et al. 2010
XMM-Newton/EPIC-pn	0.2 - 10	$\sim 3 \times 10^{-14}$	27'5 × 27'5	Watson et al. 2001
SRG/eROSITA	0.2 - 8	$\sim 10^{-13}$	0.8 deg <sup>2</sup>	Merloni et al. 2012
NICER	0.2 - 12	$\sim 8 \times 10^{-14}$	30 arcmin <sup>2</sup>	Arzoumanian et al. 2014
Insight-HXMT/LE	0.9 - 12	$\sim 1.5 \times 10^{-11}$	21 × (1'6 × 6°), 7 × (4° × 6°), 2 × (50° ~ 60° × 2° ~ 6°) or $\sim 810$ deg <sup>2</sup> total	Li et al. 2020b
SVOM/MXT	0.2 - 10	$\sim 4 \times 10^{-12}$	64' × 64'	Wei et al. 2016
XRISM/Xtend <sup>c</sup>	0.4 - 13	$\sim 6 \times 10^{-14}$	38' × 38'	XRISM Team, Private Communication
Athena/WFI	0.2 - 15	$\sim 5 \times 10^{-16}$	40' × 40'	Barcons et al. 2012
eXTP/WFM	2 - 50	$\sim 9 \times 10^{-11}$	$\sim 180^\circ \times 90^\circ$	Zhang et al. 2019
AXIS	0.1 - 10	$\sim 2 \times 10^{-16}$	144π arcmin <sup>2</sup>	Mushotzky 2018
Einstein Probe/WXT	0.5 - 4	$\sim 2 \times 10^{-11}$	3600 deg <sup>2</sup>	Yuan 2017
STAR-X	0.5 - 6	$\sim 3 \times 10^{-14}$	1 deg <sup>2</sup>	STAR-X Team, Private Communication
STROBE-X	0.2 - 12	$\sim 5 \times 10^{-14}$	4π arcmin <sup>2</sup>	Ray et al. 2019 Meidinger 2018
Lynx/HDXI	0.2 - 10	$\sim 1.5 \times 10^{-18}$	22' × 22'	The Lynx Team 2019
THESEUS/SXI	0.3 - 5	$\sim 2 \times 10^{-11}$	$\sim 0.5$ sr	Amati et al. 2021

NOTE—We use the horizontal bars to differentiate between four categories of instrument, from top to bottom we list past instruments, currently operational instruments, instruments on future missions selected for launch, and instruments on proposed missions. The list of proposed missions is not complete and it is provided to illustrate the range of capabilities of future experiments.

<sup>a</sup>0.3-10 keV; all flux limits are k-corrected to our band-of-interest assuming a fiducial  $\Gamma = 2$  spectrum. Flux limit is based on a 1 ks exposure for instruments that do pointed observations. We note that for instruments designed for higher energy observations – such as MAXI GSC or eXTP/WFM – our estimated flux limit in the 0.3 - 10 keV energy band is less secure.

<sup>b</sup>The reported Chandra 0.3 - 10 keV flux limit is estimated from recent observations

<sup>c</sup>We take the full-band Suzaku/XIS flux limit from [Miura et al. \(2008\)](#), given its sensitivity is roughly comparable to that of XRISM/Xtend (XRISM Team, Private Communication).

FRBs<sup>7</sup>), we show the luminosity distance out to which various transients can be observed vs. the fraction of the sky covered instantaneously by the instrument FOV in Figure 9. As in the rest of this work, we limit instrument depth to a maximum luminosity distance that corre-

sponds to  $z = 1$ . Needless to say, the qualitative trends captured by our Galactic and Galactic/extragalactic transient observing volume plot (Figure 9) translate to the behavior of exclusively extragalactic sources, with targeted instruments being more conducive to observing distant phenomena, while wide-field instruments have considerably shallower sky coverage.

For extragalactic transients (i.e., GRBs, SBOs, SNe, FBOTs, TDEs, and AGN), we instead examine an estimate of the number of observed events per year for each

<sup>7</sup> Though the only FRB with an apparent X-ray counterpart (FRB200428) is a Galactic source, the population of observed fast radio bursts is largely extragalactic.



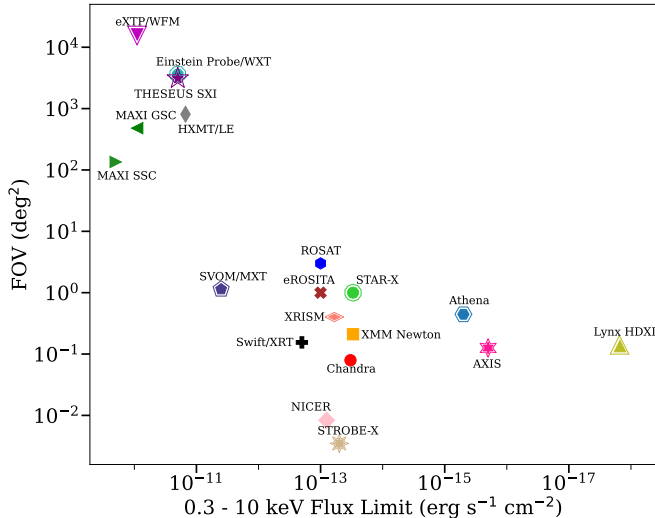


**Figure 7.** Here we show the roughly inverse relation between instrument FOV and depth with a summary of these specifications for existing and planned/proposed X-ray missions (see Table 2 for more details). We report the 1 ks 0.3-10 keV sensitivity. Upcoming/proposed instruments are highlighted by an additional marker outline.

class of phenomena broken down by instrument. Using the three-dimensional observing volumes for each instrument included in Table 2 and the same volumetric rates as in Figure 8, we construct Figure 10. The rates shown in Figure 10 are upper limits based on the most luminous event in each class. In Table 3, we report these upper limits in addition to lower limits (based on the least luminous observation in each extragalactic class in our DLPS). Both Figure 10 and Table 3 report anticipated serendipitous detection rates, assuming the instrument maintains a single static pointing on the sky and that each transient is observed as it undergoes a flare. This allows us to more readily compare instrument specifications without accounting for observing strategy. In reality, the observed rates may be much higher, particularly for survey instruments and classes of transient that can be observed months after the initial outburst (e.g., Sazonov et al. 2021).

#### 4. CONCLUSION

With the immense promise of next generation X-ray instruments on the horizon and community investment in large time-domain surveys, many more X-ray transients will be detected and studied in the coming years. We constructed a set of observational X-ray phase space plots from 284 light curves of 221 objects, which show distinctions between different transient and variable phenomena and highlight the luminosity evolution of these events. We included light curves of gamma-ray burst afterglows, supernovae, shock break-

outs, tidal disruption events and active galactic nuclei, fast blue optical transients, cataclysmic variables, magnetar flares/outbursts and fast radio bursts, cool stellar flares, X-ray binary outbursts, and ultraluminous X-ray sources comprised of observations from a range of telescopes (see Table 1 for a full list). The X-ray duration-luminosity phase space can be used to help disambiguate the nature of newly observed signals by placing them in context (even before spectroscopic or multi-wavelength follow-up, as demonstrated in Section 3.1) and to point out sparse areas of the phase space that should be the focus of future exploration.

As expected, the phase space is less populated at extremely low luminosities and extremely short durations, given the limitations of current instruments and the trade-off between FOV and sensitivity in instrument design. More sensitive imagers will provide better insight into less luminous events, but wide-field imagers will be necessary to serendipitously capture the most ephemeral signals, like those of candidate FRB counterparts. There is another, less intuitive gap in the phase space around  $L_x = 10^{34} - 10^{42}$  erg s $^{-1}$  and duration  $10^{-4} - 0.1$  days. We expect this part of the X-ray phase space to include both SBOs and magnetar flares, both of which are classes of transient that have a relative paucity of observations. Additional observations targeting this part of the phase space will not only increase the studied population of known classes of transient, but will potentially uncover yet-unidentified signals, as well.

#### ACKNOWLEDGMENTS

The authors thank the anonymous referees for comments and suggestions that significantly improved the manuscript, as well as Laura Chomiuk, Irina Zhuravleva, and Magaretha Pretorius for helpful discussions. A.P. thanks Andrey Kravtsov for the suggestion to make a preliminary classifier available. K.L.P. acknowledges support from the UK Space Agency. This work made use of data supplied by the UK Swift Science Data Centre at the University of Leicester. R.M. acknowledges partial support by the National Science Foundation under Grant No. AST-2221789 and AST-2224255, by the Heising-Simons Foundation under grant # 2021-3248. G.V. acknowledges support by Hellenic Foundation for Research and Innovation (H.F.R.I.) under the “3rd Call for H.F.R.I. Research Projects to support Postdoctoral Researchers” through the project ASTRAPE (Project ID 7802).

This research has made use of MAXI data provided by RIKEN, JAXA and the MAXI team.

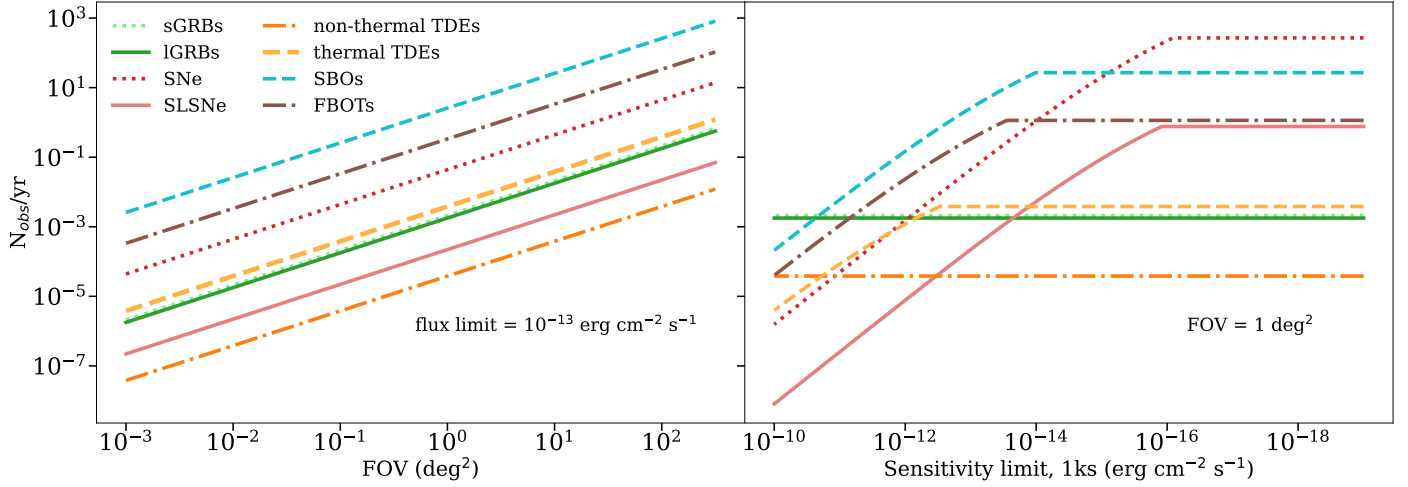


**Figure 8.** To decouple the advantages of increased field of view and sensitivity, we show extragalactic transient rates (Stone & Metzger 2016; Coppejans et al. 2020; Margutti & Chornock 2021; Ghirlanda & Salvaterra 2022) as a function of FOV with a fixed flux limit (left, sensitivity =  $10^{-13}\ erg\ s^{-1}\ cm^{-2}$ ) and the same rates as a function of sensitivity with a fixed field of view (right, FOV =  $1\ deg^2$ ). As in the rest of this work, we limit the rates to  $z \leq 1$  – which is why the number of observations per year eventually flattens with increasing sensitivity. For luminous sources, like those included here, substantial increases in the number of events detected within  $z \lesssim 1$  will primarily come from instruments with increased field of view.

*Software:* AstroPy (Astropy Collaboration et al. 2013, 2018), Matplotlib (Hunter 2007), NumPy (Harris et al. 2020), pandas (pandas development team 2020; Wes McKinney 2010), PIMMS (Mukai 1993), scikit-learn (Pedregosa et al. 2011), SciPy (Virtanen et al. 2020), WebPlotDigitizer (Rohatgi 2019)

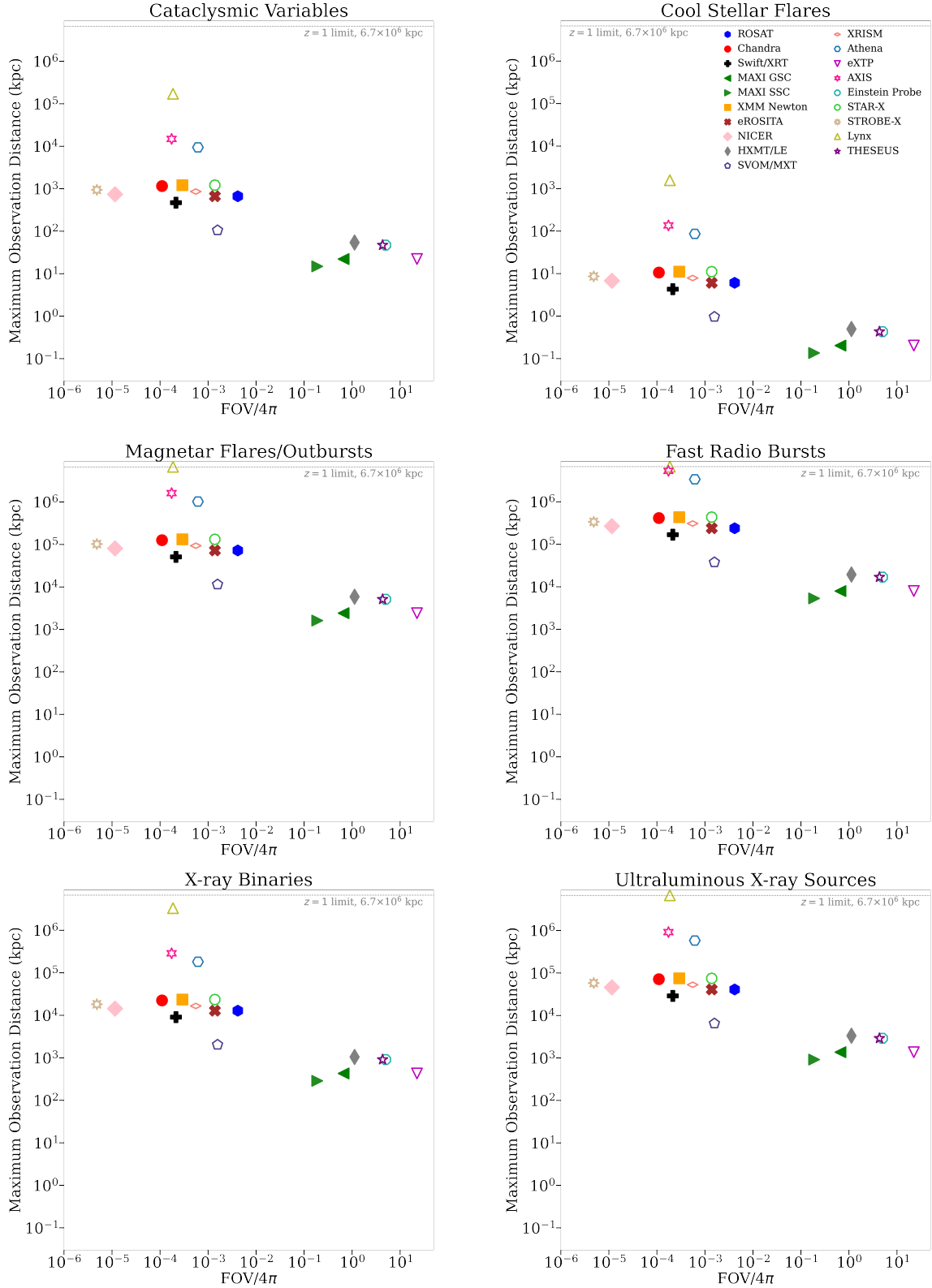


**Figure 9.** The maximum distance out to which each instrument can observe different classes of transient/variable vs. the normalized FOV (by the area of the sky). As in the rest of this work, we limit to  $z \leq 1$  ( $d_L = 6.7 \times 10^6$  kpc), which is shown by the gray dashed line. For less luminous classes of transient, the improved sensitivity from proposed/planned instruments (shown with open markers) represents an increase of up to  $\sim 3$  orders of magnitude in the distance out to which these events can be detected and observed. This significantly enlarges the potential observing volume for these signals.

**Table 3.** Estimated rate (in  $\text{yr}^{-1}$ ) of serendipitous detections of extragalactic transients in a single pointing of each soft X-ray instrument.

Instrument	sGRBs	IGRBs	SNe	SLSNe	non-thermal TDEs	thermal TDEs	SBOs	FBOTs
ROSAT	$6.28 \times 10^{-3}$ $8.98 \times 10^{-11}$	$5.34 \times 10^{-3}$ $2.19 \times 10^{-6}$	0.13 $6.32 \times 10^{-13}$	$6.63 \times 10^{-4}$ $9.96 \times 10^{-7}$	$1.15 \times 10^{-4}$ $8.28 \times 10^{-8}$	$1.15 \times 10^{-2}$ $1.59 \times 10^{-12}$	7.74 $2.85 \times 10^{-2}$	1.00 $3.62 \times 10^{-8}$
Chandra	$1.66 \times 10^{-4}$ $1.25 \times 10^{-11}$	$1.41 \times 10^{-4}$ $2.73 \times 10^{-7}$	$1.69 \times 10^{-2}$ $8.81 \times 10^{-14}$	$8.35 \times 10^{-5}$ $1.37 \times 10^{-7}$	$3.03 \times 10^{-6}$ $1.01 \times 10^{-8}$	$3.03 \times 10^{-4}$ $2.22 \times 10^{-13}$	0.68 $3.57 \times 10^{-3}$	$7.86 \times 10^{-2}$ $5.04 \times 10^{-9}$
Swift/XRT	$3.24 \times 10^{-4}$ $1.64 \times 10^{-12}$	$2.75 \times 10^{-4}$ $4.18 \times 10^{-8}$	$2.49 \times 10^{-3}$ $1.15 \times 10^{-14}$	$1.26 \times 10^{-5}$ $1.83 \times 10^{-8}$	$5.91 \times 10^{-6}$ $1.60 \times 10^{-9}$	$5.91 \times 10^{-4}$ $2.91 \times 10^{-14}$	0.18 $5.43 \times 10^{-4}$	$2.46 \times 10^{-2}$ $6.62 \times 10^{-10}$
MAXI GSC	1.00 $5.35 \times 10^{-13}$	0.854 $1.53 \times 10^{-8}$	$8.81 \times 10^{-4}$ $3.68 \times 10^{-15}$	$4.55 \times 10^{-6}$ $6.01 \times 10^{-9}$	$1.83 \times 10^{-2}$ $5.98 \times 10^{-10}$	$2.21 \times 10^{-3}$ $9.46 \times 10^{-15}$	0.12 $1.97 \times 10^{-4}$	$2.24 \times 10^{-2}$ $2.16 \times 10^{-10}$
MAXI SSC	0.283 $4.54 \times 10^{-14}$	0.240 $1.39 \times 10^{-9}$	$7.49 \times 10^{-5}$ $3.23 \times 10^{-16}$	$3.87 \times 10^{-7}$ $5.10 \times 10^{-10}$	$5.16 \times 10^{-3}$ $5.09 \times 10^{-11}$	$2.02 \times 10^{-4}$ $8.03 \times 10^{-16}$	$1.01 \times 10^{-2}$ $1.68 \times 10^{-5}$	$.95 \times 10^{-3}$ $1.83 \times 10^{-11}$
XMM Newton	$4.40 \times 10^{-4}$ $3.81 \times 10^{-11}$	$3.74 \times 10^{-4}$ $8.22 \times 10^{-7}$	$5.10 \times 10^{-2}$ $2.69 \times 10^{-13}$	$2.52 \times 10^{-4}$ $4.19 \times 10^{-7}$	$8.02 \times 10^{-6}$ $3.04 \times 10^{-8}$	$8.02 \times 10^{-4}$ $6.79 \times 10^{-13}$	2.00 $1.08 \times 10^{-2}$	0.23 $1.54 \times 10^{-8}$
eROSITA	$2.09 \times 10^{-3}$ $2.99 \times 10^{-11}$	$1.78 \times 10^{-3}$ $7.29 \times 10^{-7}$	$4.39 \times 10^{-2}$ $2.11 \times 10^{-13}$	$2.21 \times 10^{-4}$ $3.32 \times 10^{-7}$	$3.82 \times 10^{-5}$ $2.76 \times 10^{-8}$	$3.82 \times 10^{-3}$ $5.31 \times 10^{-13}$	2.58 $9.49 \times 10^{-3}$	0.334 $1.21 \times 10^{-8}$
NICER	$1.74 \times 10^{-5}$ $3.48 \times 10^{-13}$	$1.48 \times 10^{-5}$ $8.33 \times 10^{-9}$	$5.04 \times 10^{-4}$ $2.45 \times 10^{-15}$	$2.53 \times 10^{-6}$ $3.86 \times 10^{-9}$	$3.18 \times 10^{-7}$ $3.14 \times 10^{-10}$	$3.18 \times 10^{-5}$ $6.19 \times 10^{-15}$	$2.77 \times 10^{-2}$ $1.09 \times 10^{-4}$	$3.51 \times 10^{-3}$ $1.41 \times 10^{-10}$
Insight-HXMT/LE	1.70 $1.33 \times 10^{-11}$	1.44 $3.76 \times 10^{-7}$	$2.17 \times 10^{-2}$ $9.25 \times 10^{-14}$	$1.12 \times 10^{-4}$ $1.49 \times 10^{-7}$	$3.09 \times 10^{-2}$ $1.47 \times 10^{-8}$	$4.12 \times 10^{-2}$ $2.35 \times 10^{-13}$	2.73 $4.85 \times 10^{-3}$	0.50 $5.35 \times 10^{-9}$
SVOM/MXT	$2.38 \times 10^{-3}$ $1.35 \times 10^{-13}$	$2.03 \times 10^{-3}$ $3.78 \times 10^{-9}$	$2.19 \times 10^{-4}$ $9.50 \times 10^{-16}$	$1.13 \times 10^{-6}$ $1.52 \times 10^{-9}$	$4.35 \times 10^{-5}$ $1.47 \times 10^{-10}$	$1.73 \times 10^{-4}$ $2.39 \times 10^{-15}$	$2.52 \times 10^{-2}$ $4.89 \times 10^{-5}$	$4.38 \times 10^{-3}$ $5.46 \times 10^{-11}$
XRISM/Xtend	$8.40 \times 10^{-4}$ $2.58 \times 10^{-11}$	$7.14 \times 10^{-4}$ $6.01 \times 10^{-7}$	$3.66 \times 10^{-2}$ $1.82 \times 10^{-13}$	$1.83 \times 10^{-4}$ $2.85 \times 10^{-7}$	$1.53 \times 10^{-5}$ $2.26 \times 10^{-8}$	$2.94 \times 10^{-4}$ $2.39 \times 10^{-15}$	1.83 $7.84 \times 10^{-3}$	0.22 $1.04 \times 10^{-8}$
Athena WFI	$9.31 \times 10^{-4}$ $3.50 \times 10^{-8}$	$7.91 \times 10^{-4}$ $2.55 \times 10^{-4}$	19.5 $2.65 \times 10^{-10}$	$8.49 \times 10^{-2}$ $3.38 \times 10^{-4}$	$1.70 \times 10^{-5}$ $8.20 \times 10^{-6}$	$1.70 \times 10^{-3}$ $6.58 \times 10^{-10}$	12.0 3.46	0.51 $1.42 \times 10^{-5}$
eXTP/WFM	33.9 $1.80 \times 10^{-11}$	28.8 $5.16 \times 10^{-7}$	$2.97 \times 10^{-2}$ $1.24 \times 10^{-13}$	$1.53 \times 10^{-4}$ $2.03 \times 10^{-7}$	0.62 $2.02 \times 10^{-8}$	$7.46 \times 10^{-2}$ $3.19 \times 10^{-13}$	3.97 $6.66 \times 10^{-3}$	0.76 $7.28 \times 10^{-9}$
AXIS	$2.63 \times 10^{-4}$ $3.75 \times 10^{-8}$	$2.24 \times 10^{-4}$ $1.77 \times 10^{-4}$	14.4 $2.96 \times 10^{-10}$	$6.03 \times 10^{-2}$ $3.37 \times 10^{-4}$	$4.80 \times 10^{-6}$ $4.80 \times 10^{-6}$	$4.80 \times 10^{-4}$ $7.28 \times 10^{-10}$	3.38 2.42	0.14 $1.53 \times 10^{-5}$
Einstein Probe/WXT	7.54 $3.83 \times 10^{-11}$	6.41 $1.09 \times 10^{-6}$	$6.28 \times 10^{-2}$ $2.68 \times 10^{-13}$	$3.24 \times 10^{-4}$ $4.30 \times 10^{-7}$	0.14 $4.24 \times 10^{-8}$	0.13 $6.77 \times 10^{-13}$	7.99 $1.40 \times 10^{-2}$	1.48 $1.54 \times 10^{-8}$
STAR-X	$2.09 \times 10^{-3}$ $1.81 \times 10^{-10}$	$1.78 \times 10^{-3}$ $3.91 \times 10^{-6}$	0.24 $1.28 \times 10^{-12}$	$1.20 \times 10^{-3}$ $1.99 \times 10^{-6}$	$3.82 \times 10^{-5}$ $1.45 \times 10^{-7}$	$3.82 \times 10^{-3}$ $3.23 \times 10^{-12}$	9.50 $5.13 \times 10^{-2}$	1.08 $7.32 \times 10^{-8}$
STROBE-X	$7.31 \times 10^{-6}$ $2.95 \times 10^{-13}$	$6.21 \times 10^{-6}$ $6.75 \times 10^{-9}$	$4.13 \times 10^{-4}$ $2.08 \times 10^{-15}$	$2.06 \times 10^{-6}$ $3.26 \times 10^{-9}$	$1.33 \times 10^{-7}$ $2.52 \times 10^{-10}$	$1.33 \times 10^{-5}$ $5.24 \times 10^{-15}$	$1.94 \times 10^{-2}$ $8.81 \times 10^{-5}$	$2.34 \times 10^{-3}$ $1.19 \times 10^{-10}$
Lynx/HDXI	$2.82 \times 10^{-4}$ $2.62 \times 10^{-5}$	$2.39 \times 10^{-4}$ $2.39 \times 10^{-4}$	36.2 $4.85 \times 10^{-7}$	0.10 $9.97 \times 10^{-2}$	$5.14 \times 10^{-6}$ $5.14 \times 10^{-6}$	$5.14 \times 10^{-4}$ $9.33 \times 10^{-7}$	3.62 3.62	0.15 $1.13 \times 10^{-2}$
THESEUS/SXI	6.51 $3.31 \times 10^{-11}$	5.54 $9.39 \times 10^{-7}$	$5.43 \times 10^{-2}$ $2.32 \times 10^{-13}$	$2.80 \times 10^{-4}$ $3.71 \times 10^{-7}$	0.12 $3.67 \times 10^{-8}$	0.11 $5.85 \times 10^{-13}$	6.90 $1.21 \times 10^{-2}$	1.28 $1.33 \times 10^{-8}$

NOTE—For each instrument we show an upper (top) and lower (bottom) limit for the serendipitous observation rate, assuming that the instrument remains pointed at the same portion of the sky and takes 1ks exposures

The upper limit is based on the observing volume calculated for the most luminous observation of an event in that class, while the lower limit is based on the observing volume calculated for the least luminous observation of an event in that class. As in Table 2, we separate past, present, planned, and proposed instruments with horizontal lines.

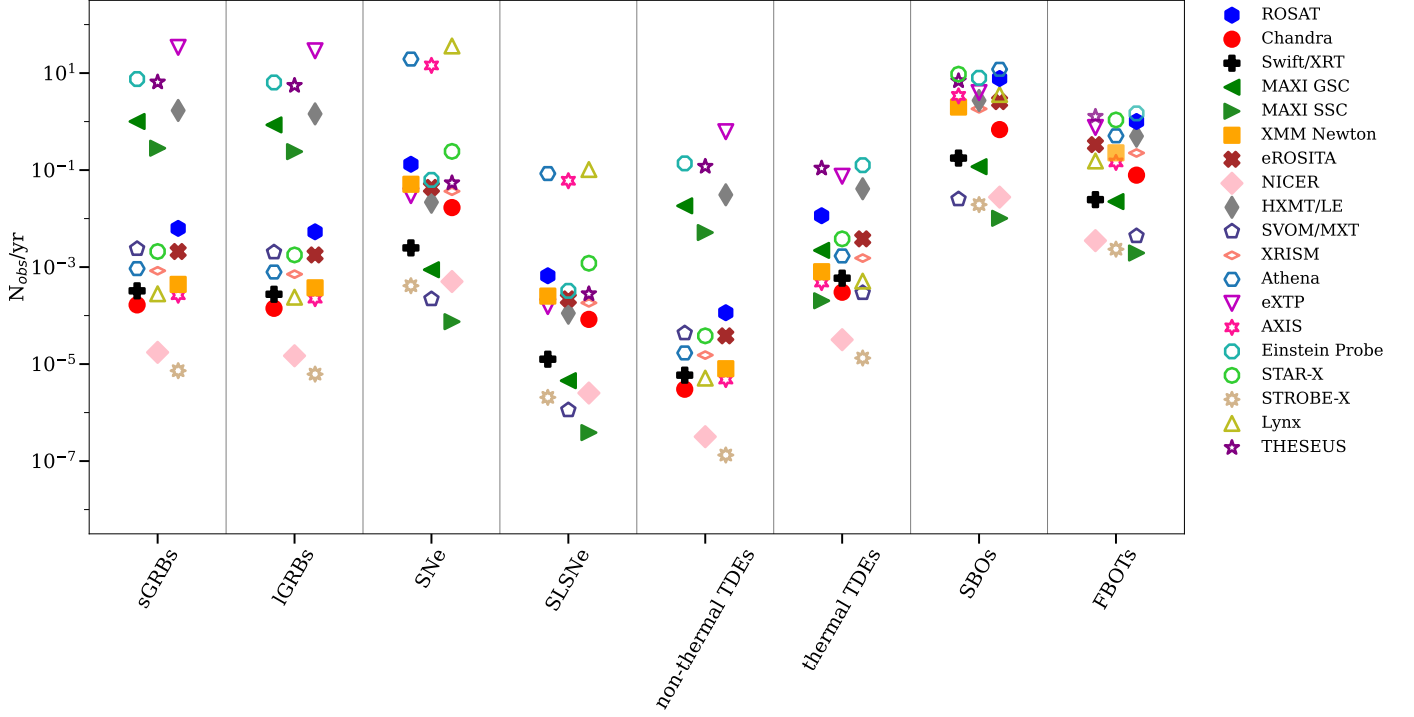


**Figure 10.** Estimates of the number of serendipitous observations expected per year for transients with a variety of different instruments based on the volumetric rates of the phenomena and the observing volume of each instrument. The comoving depth out to which each instrument can observe each class of phenomenon is calculated based on the peak observed luminosity of each phenomenon, making the assumption that we have already detected the most intrinsically luminous signal from each type of transient. We take rates from Stone & Metzger (2016), Coppejans et al. (2020), Margutti & Chornock (2021), and Ghirlanda & Salvaterra (2022). For the GRBs, both long and short, we apply a beaming correction assuming a jet opening angle  $\sim 3^\circ$ . See Table 3 for more details. As with the rest of the paper, the number of expected observations per year is quoted out to  $z = 1$ , corresponding to  $d_L \sim 6700$  Mpc or  $d_{com} \sim 3350$  Mpc. For each class of transient shown here, next-generation instruments (open markers) represent an increase in the anticipated number of events observed per year. In the case of more intrinsically luminous transients, this is due to increased FOV, while less luminous classes benefit more from improved sensitivity (see Figure 8).

## APPENDIX

## A. DATA

We list here all of the events included in the paper. For each event, we also provide coordinates, distance, and references, and, where applicable, we provide sub-classification. For GRBs, we also list redshift and  $T_{90}$ . These data are available on GitHub (see Section 2), with a few limited exceptions, which are marked clearly in the tables below. Quoted distances are luminosity distances for the cosmology indicated in Section 1.

## B. THE TRUE OBSERVER'S PHASE SPACE: FLUX VS. DURATION

While the luminosity X-ray phase space is very instructive for understanding which physical phenomena are poorly captured by current instruments, it does little to reinforce the role that instrument sensitivity plays in determining which phenomena are detected. We show a purely observational duration-flux phase space in Figure 11.

Future missions will improve substantially on current sensitivity limits. This will open up an innately new area of the low luminosity parameter space, significantly extending the depth out to which known classes of transients can be detected and potentially revealing the existence of yet-unknown intrinsically faint signals.

## C. THE SCHEMATIC DLPS

In addition to the phase space plots that are populated with real light curves, we offer a schematic version of the DLPS in Figure 12. We determine the bounds of the colored blocks based on the specific location of our collected light curves and use these regions as a guide to generate focused subplots that show each (sub)class of transient in greater detail, rather than in the broader context of other signals in the DLPS.

**Table A1.** Gamma-ray Bursts

Name	Type	$T_{90}$ (s)	RA	Dec	z	Distance (kpc)	References
GRB980425A	subluminous	22.0	19:35:03	-52:50:46	0.0085	$2.7 \times 10^4$	Pian et al. 2000; Kouveliotou et al. 2004
GRB031203A	subluminous	30	08:02:30	-39:51:03	0.105	$4.9 \times 10^5$	Sazonov et al. 2004; Watson et al. 2004
GRB050509B	short	0.073	12:36:18	+29:01:24	0.225	$1.1 \times 10^6$	Evans et al. 2007, 2009
GRB050724	short	3.00	16:24:44	-27:32:28	0.258	$1.3 \times 10^6$	Evans et al. 2007, 2009
GRB051221A	short	1.400	21:54:49	+16:53:27	0.5465	$3.2 \times 10^6$	Evans et al. 2007, 2009
GRB060218A	subluminous	2100	09:09:31	+33:08:20	0.0331	$1.5 \times 10^5$	Evans et al. 2007, 2009
GRB061006	short	0.42	07:24:08	-79:11:55	0.438	$2.4 \times 10^6$	Evans et al. 2007, 2009
GRB061210	short	85.0	09:38:05	+15:37:17	0.4095	$2.3 \times 10^6$	Evans et al. 2007, 2009
GRB061217	short	0.210	10:41:39	-21:07:22	0.827	$5.3 \times 10^6$	Evans et al. 2007, 2009
GRB070714B	short	3.0	03:51:22	+28:17:51	0.923	$6.1 \times 10^6$	Evans et al. 2007, 2009
GRB070724A	short	0.4	01:51:14	-18:35:39	0.457	$2.6 \times 10^6$	Evans et al. 2007, 2009
GRB071227	short	1.8	03:52:31	-55:59:03	0.383	$2.1 \times 10^6$	Evans et al. 2007, 2009
GRB080905A	short	1.0	19:10:39	-18:51:55	0.1218	$5.7 \times 10^5$	Evans et al. 2007, 2009
GRB090510A	short	0.3	22:14:13	-26:35:51	0.903	$5.9 \times 10^6$	Evans et al. 2007, 2009
GRB100117A	short	0.3	00:45:05	-01:35:42	0.92	$6.0 \times 10^6$	Evans et al. 2007, 2009
GRB100316D	subluminous	292.8	07:10:31	-56:15:20	0.059	$2.7 \times 10^5$	Evans et al. 2007, 2009
GRB100816A	short	2.9	23:26:58	+26:34:43	0.8049	$5.1 \times 10^6$	Evans et al. 2007, 2009
GRB101219A	short	0.6	04:58:20	-02:32:23	0.718	$4.4 \times 10^6$	Evans et al. 2007, 2009
GRB101225A	ultralong	1088	00:00:47	+44:36:01	0.847	$5.5 \times 10^6$	Evans et al. 2007, 2009
GRB141212A	short	0.30	02:36:30	+18:08:49	0.596	$3.5 \times 10^6$	Evans et al. 2007, 2009
GRB141225A	long	40.24	09:15:07	+33:47:31	0.915	$6.0 \times 10^6$	Evans et al. 2007, 2009
GRB150101B	short	0.08	12:32:05	-10:56:01	0.134	$6.4 \times 10^5$	Evans et al. 2007, 2009
GRB150323A	long	149.6	08:32:43	+45:27:53	0.593	$3.5 \times 10^6$	Evans et al. 2007, 2009
GRB150514A	long	10.8	04:59:30	-60:58:07	0.807	$5.1 \times 10^6$	Evans et al. 2007, 2009
GRB150518A	subluminous	–	15:36:48	+16:19:47	0.256	$1.3 \times 10^6$	Evans et al. 2007, 2009
GRB150727A	long	88	13:35:53	-18:19:32	0.313	$1.6 \times 10^6$	Evans et al. 2007, 2009
GRB150818A	long	123.3	15:21:25	+68:20:31	0.282	$1.5 \times 10^6$	Evans et al. 2007, 2009
GRB150821A	long	172.1	22:47:39	-57:53:38	0.755	$4.7 \times 10^6$	Evans et al. 2007, 2009
GRB151027A	long	129.69	18:09:57	+61:21:12	0.81	$5.2 \times 10^6$	Evans et al. 2007, 2009
GRB160131A	long	325	05:12:40	-07:03:00	0.972	$6.5 \times 10^6$	Evans et al. 2007, 2009
GRB160314A	long	8.73	07:31:10	+16:59:57	0.726	$4.9 \times 10^6$	Evans et al. 2007, 2009
GRB160425A	long	304.58	18:41:19	-54:21:36	0.555	$3.2 \times 10^6$	Evans et al. 2007, 2009
GRB160623A	long	13.5	21:01:12	+42:13:15	0.367	$2.0 \times 10^6$	Evans et al. 2007, 2009
GRB160624A	short	0.2	22:00:46	+29:38:38	0.483	$2.7 \times 10^6$	Evans et al. 2007, 2009
GRB160804A	long	130	14:46:31	+09:59:56	0.736	$4.6 \times 10^3$	Evans et al. 2007, 2009
GRB160821B	short	0.48	18:39:55	+62:23:30	0.16	$7.7 \times 10^5$	Evans et al. 2007, 2009
GRB161129A	long	35.53	21:04:55	+32:08:05	0.645	$3.9 \times 10^6$	Evans et al. 2007, 2009
GRB161219B	long	6.94	06:06:5	-26:47:30	0.1475	$7.1 \times 10^5$	Evans et al. 2007, 2009
GRB170519A	long	216.4	10:53:42	+25:22:27	0.818	$5.2 \times 10^6$	Evans et al. 2007, 2009
GRB170607A	long	23.0	00:29:28	+09:14:36	0.557	$3.3 \times 10^6$	Evans et al. 2007, 2009
GRB170714A	ultralong	1000	02:17:24	+01:59:29	0.793	$5.0 \times 10^6$	Evans et al. 2007, 2009
GRB170817A	short	2.0	13:09:48	-23:22:53	0.0099	$4.3 \times 10^4$	Hajela et al. 2019, 2020
GRB171010A	long	70.3	04:26:19	-10:27:48	0.3285	$1.7 \times 10^6$	Evans et al. 2007, 2009
GRB171205A	subluminous	189.4	11:09:39	-12:35:19	0.0368	$1.6 \times 10^5$	Evans et al. 2007, 2009
GRB180404A	long	35.2	05:34:12	-37:10:05	1.000	$6.7 \times 10^6$	Evans et al. 2007, 2009
GRB180703A	long	20.9	00:24:28	-67:18:18	0.6678	$4.0 \times 10^6$	Evans et al. 2007, 2009
GRB180720B	long	51.1	00:02:07	-02:55:08	0.654	$4.0 \times 10^6$	Evans et al. 2007, 2009
GRB180728A	long	8.68	16:54:16	-54:02:40	0.117	$5.5 \times 10^5$	Evans et al. 2007, 2009
GRB190114C	long	361.5	03:38:01	-26:56:48	0.425	$2.4 \times 10^6$	Evans et al. 2007, 2009
GRB190829A	long	63	02:58:10	-08:57:30	0.0785	$3.6 \times 10^5$	Evans et al. 2007, 2009
GRB191019A	long	64.35	22:40:06	-17:19:41	0.248	$1.3 \times 10^6$	Evans et al. 2007, 2009
GRB221009A	long	327	19:12:50	+19:43:48	0.151	$7.2 \times 10^5$	Evans et al. 2007, 2009; de Ugarte Postigo et al. 2022

**Table A2.** Shock Breakouts

Name	Type	RA	Dec	Distance (kpc)	References
GRB980425A	stellar surface	19:35:03	-52:50.46	$3.7 \times 10^4$	Pian et al. 2000; Kouveliotou et al. 2004
GRB031203A	stellar surface	08:02:30	-39:51:03	$4.9 \times 10^5$	Sazonov et al. 2004; Watson et al. 2004
GRB060218A	stellar surface	03:21:40	+16:52:02	$1.5 \times 10^5$	Evans et al. 2007, 2009
SN2008D (GRB080109A)	wind	09:09:31	+33:08:20	$2.7 \times 10^4$	Soderberg et al. 2008
GRB100316D	stellar surface	07:10:31	-56:15:20	$2.7 \times 10^5$	Evans et al. 2007, 2009
GRB150518A	stellar surface	15:36:48	+16:19:47	$1.3 \times 10^6$	Evans et al. 2007, 2009
GRB171205A	stellar surface	11:09:39	-12:35:19	$1.6 \times 10^5$	Evans et al. 2007, 2009

NOTE—Subluminous GRBs are considered candidates for stellar surface shock breakouts. We include them here under that assumption.

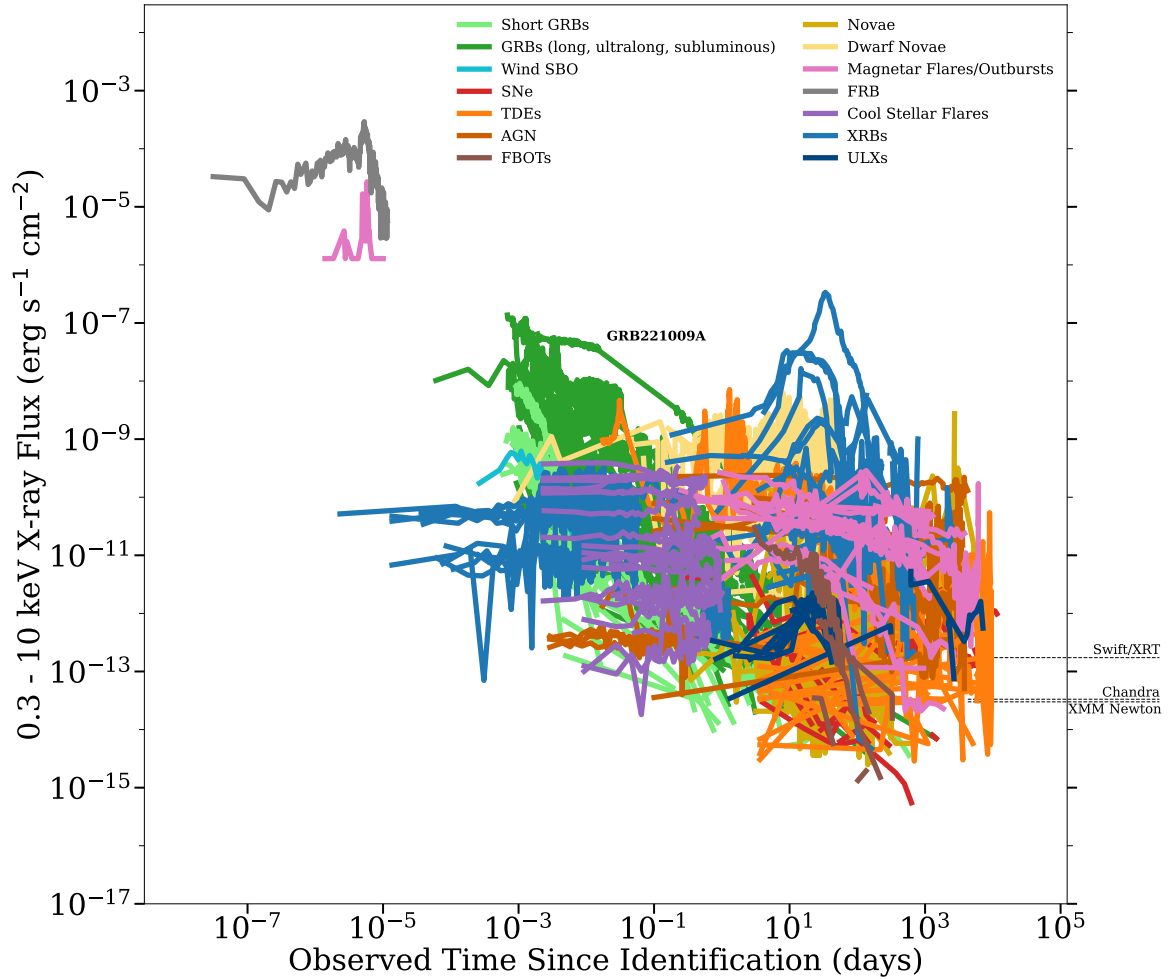


**Figure 11.** The duration-flux phase space of X-ray transient and variable phenomena. To demonstrate the limitations of current observatories, we mark the 0.3-10 keV flux limit for a handful of instruments, assuming a 1ks integration time.



**Table A3.** Supernovae

Name	Type	RA	Dec	Distance (kpc)	References
SN1978K	II	03:17:39	-66:33:03	$4.5 \times 10^3$	Raffaella Margutti, Private Communication
SN1981K	II	12:18:59	+47:19:31	$7.2 \times 10^3$	Immler et al. 2007b
SN1987A	IIPec	05:35:28	-69:16:11	50	Haberl et al. 2006; Heng et al. 2008; Sturm et al. 2010
SN1993J	I Ib	09:55:25	+69:01:14	$2.6 \times 10^3$	Chandra et al. 2009
SN1995N	I In	14:49:28	-10:10:14	$2.4 \times 10^4$	Zampieri et al. 2005
SN1996cr	I In	14:13:10	-65:20:45	$3.8 \times 10^3$	Bauer et al. 2008
SN1998bw	Ib/c	19:35:03	-52:50:46	$3.8 \times 10^4$	Kouveliotou et al. 2004
SN1999em	IIP	04:41:27	-02:51:45	$7.8 \times 10^3$	Pooley et al. 2002
SN1999gi	IIP	10:18:17	+41:26:28	$8.7 \times 10^3$	Schlegel 2001
SN2001ig	II	22:57:31	-41:02:26	$1.1 \times 10^4$	Schlegel & Ryder 2002
SN2002ap	Ib/c	01:36:24	+15:45:13	$1.0 \times 10^4$	Soria et al. 2004
SN2003bg	Ic/pec	04:10:59	-31:24:50	$1.9 \times 10^4$	Soderberg et al. 2006
SN2004et	II	20:35:25	+60:07:18	$5.5 \times 10^3$	Misra et al. 2007
SN2005ip	I In	09:32:06	+08:26:44	$3.0 \times 10^4$	Immler & Pooley 2007
SN2005kd	I In	04:03:17	+71:43:19	$6.4 \times 10^4$	Immler et al. 2007c; Pooley et al. 2007
SN2006bp	IIP	11:53:56	+52:21:09	$1.5 \times 10^4$	Immler et al. 2007e
SN2006jc	Ibc	09:17:21	+41:54:33	$2.4 \times 10^4$	Immler et al. 2008
SN2006jd	I Ib/I In	08:02:07	+00:48:32	$7.9 \times 10^4$	Immler et al. 2007a
SN2007pk	I In	01:31:47	+33:36:54	$7.1 \times 10^4$	Immler et al. 2007d
SN2008M	II	06:21:41	-59:43:45	$3.7 \times 10^4$	Immler 2010
SN2008ax	I Ib	12:30:41	+41:38:16	$8.0 \times 10^3$	Roming et al. 2009
SN2008ij	II	18:19:52	+74:33:55	$2.1 \times 10^4$	Immler et al. 2009
SN2009gj	I Ib	00:30:29	-33:12:56	$1.8 \times 10^4$	Immler & Russell 2009
SN2009mk	I Ib	00:06:21	-41:29:00	$2.1 \times 10^4$	Russell & Immler 2010
SN2010F	II	10:05:21	-34:13:21	$3.9 \times 10^4$	Russell et al. 2010
SN2010jl	I In	09:42:53	+09:29:42	$4.9 \times 10^4$	Immler et al. 2010; Chandra et al. 2015
SN2011dh	I Ib	13:30:05	+47:10:11	$7.3 \times 10^3$	Soderberg et al. 2012
SN2011ja	IIP	13:05:11	-49:31:27	$3.0 \times 10^3$	Chakraborti et al. 2013
SN2013by	IIL/I In	16:59:02	-60:11:42	$1.5 \times 10^4$	Margutti et al. 2013
SN2013ej	IIP/IIL	01:36:48	+15:45:31	$9.6 \times 10^3$	Chakraborti et al. 2016
SN2014C	Ib/I In	22:37:06	+34:24:32	$1.5 \times 10^4$	Brethauer et al. 2022
SN2018gk	I Ib/SL	16:35:54	+40:01:58	$1.4 \times 10^5$	Bose et al. 2021
SN2018bsz <sup>a</sup>	I/SL	16:09:39	-32:03:46	$1.1 \times 10^5$	Matthews et al. in prep
SN2019ehk	Ca-rich	12:22:56	+15:49:34	$1.6 \times 10^4$	Jacobson-Galán et al. 2020
SN2021gno	Ca-rich	12:12:10	+13:14:57	$3.05 \times 10^4$	Jacobson-Galán et al. 2022

NOTE—Type “SL” denotes superluminous supernovae. Additional X-ray SNe observations may be, or may become, available in SNaX ([kronos.uchicago.edu/snax](https://kronos.uchicago.edu/snax); Ross & Dwarkadas 2017; Nisenoff et al. 2020), which is a moderated database serving as a repository for user-uploaded X-ray observations of supernovae.

<sup>a</sup>These data are not shared in the GitHub repository.

**Table A4.** Tidal Disruption Events and Active Galactic Nuclei

Name	Type	RA	Dec	Distance (kpc)	References
PKS 2155-304	AGN	21:58:52.	-30:13:32	$5.4 \times 10^5$	Auchettl et al. 2018
3C 273	AGN	12:29:07	+02:03:09	$7.6 \times 10^5$	Auchettl et al. 2018
NGC 4395	AGN	12:25:49	+33:32:49	$4.7 \times 10^3$	Auchettl et al. 2018
3C 279	AGN	12:56:11	-05:47:22	$3.1 \times 10^6$	Auchettl et al. 2018
3C 345	AGN	16:42:59	+39:48:37	$3.5 \times 10^6$	Auchettl et al. 2018
MKN 335	AGN	00:06:20	+20:12:11	$1.1 \times 10^5$	Auchettl et al. 2018
CGC 229-10 (Zw 299-015)	AGN	16:41:09	+61:19:35	$8.7 \times 10^4$	Auchettl et al. 2018
PS10jh	thermal TDE	16:09:28	+53:40:23	$8.2 \times 10^5$	Auchettl et al. 2017
ASASSN-14ae	thermal TDE	11:08:40	+34:05:52	$2.0 \times 10^5$	Auchettl et al. 2017
ASASSN-14li	thermal TDE	12:48:15	+17:46:26	$9.0 \times 10^4$	Miller et al. 2015; Brown et al. 2017 Auchettl et al. 2017; Bright et al. 2018
ASASSN-15oi	thermal TDE	20:39:09	-30:45:21	$2.2 \times 10^5$	Auchettl et al. 2017; Holoien et al. 2018
Swift 1644+57	non-thermal TDE	16:44:49	+57:34:51	$1.9 \times 10^6$	Mangano et al. 2016; Auchettl et al. 2017
ASASSN-19bt	non-thermal TDE	07:00:11	-66:02:25	$1.15 \times 10^5$	Holoien et al. 2019
Swift J2058.4+0516 <sup>a</sup>	non-thermal TDE	20:58:20	+05:13:32	$1 \times 10^7$	Auchettl et al. 2017
SDSS J131122.15-012345.6	thermal TDE	13:11:22	-01:23:46	$9.0 \times 10^5$	Auchettl et al. 2017
SDSS J132341.97+482701.3	thermal TDE	13:23:42	+48:27:01	$4.0 \times 10^5$	Auchettl et al. 2017
SDSS J1201+3003	thermal TDE	12:01:36	+30:03:06	$7.1 \times 10^5$	Auchettl et al. 2017
WINGS J1348	thermal TDE	13:48:51	+26:35:06	$2.8 \times 10^5$	Auchettl et al. 2017
RBS 1032	thermal TDE	11:47:27	+49:42:57	$1.1 \times 10^5$	Auchettl et al. 2017
3XMM J1521+0749	thermal TDE	11:47:27	+49:42:58	$8.9 \times 10^5$	Auchettl et al. 2017
GSN 069	AGN/QPE	01:19:09	-34:11:30	$7.86 \times 10^4$	Miniutti et al. 2019
2MASX J0249	thermal TDE	02:49:17	-04:12:52	$8.0 \times 10^4$	Auchettl et al. 2017
IGR J17361-4441	thermal TDE	17:36:17	-44:44:06	$1.8 \times 10^5$	Auchettl et al. 2017
NGC 247	thermal TDE	00:47:09	-20:45:37	2240	Auchettl et al. 2017
OGLE 16aaa	thermal TDE	01:07:21	-64:16:21	$8.1 \times 10^5$	Auchettl et al. 2017
PTF-10iya	thermal TDE	14:38:41	+37:39:33	$1.2 \times 10^6$	Auchettl et al. 2017
XMMSL1 J0740-85	thermal TDE	07:40:08	-85:39:31	$7.4 \times 10^4$	Auchettl et al. 2017

<sup>a</sup>Though Swift J2058.4+0516 is at  $z \sim 1$ , we include its light curve anyway due to the relative paucity of non-thermal TDE observations and the uncertainty on its distance estimate.

**Table A5.** Fast Blue Optical Transients

Name	RA	Dec	Distance (kpc)	References
CSS161010	04:58:34	-08:18:04	$1.5 \times 10^5$	Coppejans et al. 2020
AT2018cow	16:16:00	+22:16:05	$6.0 \times 10^4$	Margutti et al. 2019
AT2020xnd	22:20:02	-02:50:25	$1.2 \times 10^6$	Bright et al. 2022
AT2020mrf	15:47:54	+44:29:07	$6.37 \times 10^5$	Yao et al. 2022
AT2022tsd	03:20:11	+08:44:56	$1.3 \times 10^6$	Schulze et al. 2022; Matthews et al. 2022; Matthews & Margutti 2023

**Table A6.** Cataclysmic Variables

Name	Type	RA	Dec	Distance (kpc)	References
V838 Her	Nova	18:46:32 +	12:14:01	3.4	Mukai et al. 2008
V1974 Cyg	Nova	20:30:32	+52:37:51	1.9	Mukai et al. 2008
V351 Pup	Nova	08:11:38	-35:07:30	4.7	Mukai et al. 2008
V382 Vel	Nova	10:44:48	-52:25:31	1.7	Mukai et al. 2008
N LMC 2000 <sup>a</sup>	Nova	05:25:02	-70:14:17	55	Mukai et al. 2008
V4633 Sgr	Nova	18:21:40	-27:31:37	8.9	Mukai et al. 2008
V5116 Sgr	Nova	18:17:51	-30:26:31	11.3	Mukai et al. 2008
V1663 Aql	Nova	19:05:12	+05:14:12	5.5	Mukai et al. 2008
V477 Sct	Nova	18:38:43	-12:16:16	11	Mukai et al. 2008
V382 Nor	Nova	16:19:45	-51:34:53	13.8	Mukai et al. 2008
RS Oph	Nova	17:50:13	-06:42:28	1.6	Page et al. 2020
V2362 Cyg	Nova	21:11:32	+44:48:04	7.2 - 15.8	Poggiani 2009; Page et al. 2020
V1280 Sco	Nova	16:57:41	-32:20:36	1.6	Chesneau et al. 2008; Page et al. 2020
V1281 Sco	Nova	16:56:59	-35:21:50	25.9	Kantharia 2017; Page et al. 2020
V458 Vul	Nova	19:54:25	+20:52:53	8.5	Page et al. 2020
V597 Pup	Nova	08:16:18	-34:15:25	3	Worpel et al. 2020; Page et al. 2020
V2468 Cyg	Nova	19:58:34	+29:52:12	5.6	Raj et al. 2015; Page et al. 2020
V2491 Cyg	Nova	19:43:02	+32:19:14	10.5 - 14	Darnley et al. 2011; Page et al. 2020
HV Cet (CSS081007)	Nova	03:05:59	+05:47:16	4.45	Page et al. 2020
LMC 2009a	Nova	05:04:44	-66:40:12	50	Page et al. 2020
V2672 Oph	Nova	17:38:20	-26:44:14	19	Munari et al. 2011; Page et al. 2020
KT Eri	Nova	04:47:54	-10:10:43	6.3	Raj et al. 2013; Page et al. 2020
U Sco	Nova	16:22:31	-17:52:43	12	Schaefer 2010; Page et al. 2020
V407 Cyg	Nova	21:02:10	+45:46:33	2.7	Page et al. 2020
T Pyx	Nova	09:04:42	-32:22:48	3.185	Schaefer 2018; Page et al. 2020
LMC 2012	Nova	04:54:57	-70:26:56	50	Page et al. 2020
V959 Mon	Nova	06:39:39	+05:53:53	1.4	Page et al. 2020; Li et al. 2020a
SMC 2012	Nova	00:32:34	-74:20:15	61	Page et al. 2020
V339 Del	Nova	20:23:31	+20:46:04	2.1	Page et al. 2020; Li et al. 2020a
V1369 Cen	Nova	13:54:45	-59:09:04	2.0	Page et al. 2020; Li et al. 2020a
V745 Sco	Nova	17:55:22	-33:14:59	7.8	Schaefer 2010; Page et al. 2020
V1534 Sco	Nova	17:15:47	-31:28:30	8.8	Hachisu & Kato 2018; Page et al. 2020
V1535 Sco	Nova	17:03:26	-35:04:18	8.5	Linford et al. 2017; Page et al. 2020
V5668 Sgr	Nova	18:37:40	-29:04:03	2.0	Page et al. 2020; Li et al. 2020a
LMC 1968-12a	Nova	05:09:58	-71:39:53	50	Page et al. 2020
V407 Lup	Nova	15:29:02	-44:49:41	~ 10	Aydi et al. 2018; Page et al. 2020
SMCN 2016-10a	Nova	01:06:03	-74:47:16	61	Page et al. 2020
V549 Vel	Nova	08:50:30	-47:45:28	0.560	Page et al. 2020; Li et al. 2020a
SS Cyg	Dwarf Nova	21:42:43	+43:35:10	0.115	Wheatley et al. 2003; McGowan et al. 2004; Pala et al. 2020
GW Lib	Dwarf Nova	15:19:55	-25:00:25	0.113	Byckling et al. 2009; Neustroev et al. 2018; Pala et al. 2020
SSS J122221.7-311525	Dwarf Nova	12:22:22	-31:15:24	0.275	Neustroev et al. 2018

NOTE—We include only the dwarf novae with well-observed X-ray brightening during their optical outbursts.

<sup>a</sup>We quote the 55 kpc distance assumed by Mukai et al. (2008) since these light curves are from that paper and presented as luminosity vs. time. Other novae in the LMC are listed with a more recently revised distance (Pietrzyński et al. 2013) as those data were initially presented as flux vs. time.

**Table A7.** Magnetar Flares/Outbursts + FRBs

Name	Type	RA	Dec	Distance (kpc)	References
1E161348-5055	Outburst	16:17:33	-51:02:00	3.3	Rea et al. 2016; Esposito et al. 2019
SGR 1627-41	Outburst	16:35:52	-47:35:12	11	Coti Zelati et al. 2018
1E2259+586	Outburst	23:01:08	+58:52:44	3.2	Coti Zelati et al. 2018
XTE J1810-197	Outburst	18:09:51	-19:43:52	3.5	Coti Zelati et al. 2018
SGR 1806-20	Outburst	18:08:39	-20:24:40	8.7	Coti Zelati et al. 2018
CXOU J1647-4552	Outburst	16:47:10	-45:52:17	4	Coti Zelati et al. 2018
SGR 0501+4516	Outburst	05:01:08	+45:16:31	1.5	Coti Zelati et al. 2018
1E1547.0-5408	Outburst	15:50:54	-54:18:24	4.5	Coti Zelati et al. 2018
SGR 0418+5729	Outburst	04:18:34	+57:32:23	2	Coti Zelati et al. 2018
SGR 1833-0832	Outburst	18:33:46	-08:32:13	10	Coti Zelati et al. 2018
Swift J1822.3-1606	Outburst	18:22:18	-16:04:27	1.6	Coti Zelati et al. 2018
Swift J1834.9-0846	Outburst	18:34:53	-08:45:41	4.2	Coti Zelati et al. 2018
1E1048.1-5937	Outburst	10:50:09	-59:53:20	9	Coti Zelati et al. 2018
SGR J1745-2900	Outburst	17:45:40	-29:00:30	8.3	Coti Zelati et al. 2018
SGR 1935+2154 (FRB 200428) <sup>a</sup>	FRB	19:34:56	+21:53:48	4.4	Li et al. 2021
SGR 1935+2154	IF/SB				Matsuoka et al. 2009; Sugawara et al. 2020

NOTE—As with the other variable classes, one listed object may correspond to multiple light curves within our X-ray phase space. To remain consistent with our discussion in Section 2.7, we categorize magnetar transience as either intermediate flare/short burst (IF/SB in the table) or outburst. Quiescent behavior is shown for the listed outbursts, with  $L_x$  taken from Olausen & Kaspi (2014).

<sup>a</sup>SGR 1935+2154 is believed to be a fast radio burst X-ray counterpart with a magnetar progenitor. For that reason, we include it with our sample of magnetar flares and outbursts. These data (both the IF/SB and FRB counterpart) are from the same burst forest in April 2020 for direct comparison. We adopt a distance of 4.4 kpc from Mereghetti et al. (2020).

**Table A8.** Cool Stellar Flares

Name	RA	Dec	Distance (kpc)	References
UY Scl	00:14:46	-39:14:36	0.1372	<a href="#">Pye et al. 2015</a>
HD 1165	00:16:53	+81:39:49	0.0332	<a href="#">Pye et al. 2015</a>
HD 14716	02:16:04	-73:50:43	0.062	<a href="#">Pye et al. 2015</a>
CC Eri	02:34:23	-43:47:47	0.0116	<a href="#">Pye et al. 2015</a>
CD-53 544	02:41:47	-52:59:52	0.028	<a href="#">Pye et al. 2015</a>
SDSS J033815.04+002926.0	03:38:15	+00:29:26	0.7099	<a href="#">Pye et al. 2015</a>
V471 Tau	03:50:25	+17:14:47	0.0441	<a href="#">Pye et al. 2015</a>
2MASS J04072181-1210033	04:07:22	-12:10:03	0.3957	<a href="#">Pye et al. 2015</a>
V410 Tau	04:18:31	+28:27:16	0.0982	<a href="#">Pye et al. 2015</a>
T Tau	04:21:59	+19:32:06	0.1825	<a href="#">Pye et al. 2015</a>
HD 285845	04:31:25	+18:16:17	0.090	<a href="#">Pye et al. 2015</a>
HD 283810	04:40:09	+25:35:33	0.060	<a href="#">Pye et al. 2015</a>
HD 268974	05:05:27	-67:43:14	0.9174	<a href="#">Pye et al. 2015</a>
AB Dor	05:28:45	-65:26:55	0.0152	<a href="#">Pye et al. 2015</a>
SV Cam	06:41:19	+82:16:02	0.088	<a href="#">Pye et al. 2015</a>
pi.01 UMa	08:39:12	+65:01:15	0.0144	<a href="#">Pye et al. 2015</a>
2MASS J13141103-1620235	13:14:11	-16:20:24	0.5161	<a href="#">Pye et al. 2015</a>
1RXS J231628.7+790531	23:16:31	+79:05:36	0.055	<a href="#">Pye et al. 2015</a>

NOTE—As with the progenitors of other classes of recurrent outburst, individual flares are shown separately in our X-ray phase space, so some of the objects listed may correspond to a number of unique light curves.

**Table A9.** X-ray Binary Outbursts and Ultraluminous X-ray Sources

Name	Type	RA	Dec	Distance (kpc)	Reference
4U 0352-309 (X Persei)	HMXRB	03:55:23	+31:02:45	1	La Palombara & Mereghetti 2007
XMMU J004243.6+412519	ULX	00:42:44	+41:25:19	778	Middleton et al. 2013
RX J0209.6-7427	HMXRB	02:09:34	-74:27:12	55	Vasilopoulos et al. 2020b
PSR J1023+0038 <sup>a</sup>	LMXRB	10:23:48	+00:38:41	1.37	Bogdanov et al. 2015
IGR J01217-7257 (SXP 2.16)	HMXRB	01:21:41	-72:57:22	62	Boon et al. 2017; Vasilopoulos et al. 2017a
SXP 15.6	HMXRB	00:48:55	-73:49:46	62	Vasilopoulos et al. 2017b
CG X-1	ULX	14:13:12	-65:20:14	4200	Qiu et al. 2019
M51 ULX-7	ULX	13:30:01	+47:13:44	8580	Vasilopoulos et al. 2020a
NGC 925 ULX-3	ULX	02:27:20	+33:34:13	9560	Earnshaw et al. 2020
Aql X-1 <sup>b</sup>	LMXRB	19:11:16	+00:35:06	~ 5	López-Navas et al. 2020
GX 339-4 <sup>b</sup>	LMXRB	17:02:49	-48:47:23	8	Kong et al. 2000; Corbel et al. 2013
MAXI J1659-152	LMXRB	16:59:02	-15:15:29	6	Jonker et al. 2012
4U J1907+09	HMXRB	19:09:41	+09:48:25	5	Ferrigno et al. 2022
IGR J16393-4643	HMXRB	16:39:06	-46:42:14	12	Ferrigno et al. 2022
IGR J17503-2636	HMXRB	17:50:18	-26:36:17	10	Ferrigno et al. 2022
IGR J19140+0951	HMXRB	19:14:04	+09:52:58	2.8	Ferrigno et al. 2022
Swift J0243.6+6124	HMXRB	02:43:40	+61:26:04	7	Wilson-Hodge et al. 2018; Chatzis et al. 2022
RX J0520.5-6932	HMXRB	05:20:31	-69:31:55	50	Vasilopoulos et al. 2014
SMC X-2	HMXRB	00:54:33	-73:41:01	62	Lutovinov et al. 2017
SMC X-3	HMXRB	00:52:06	-72:26:04	62	Koliopanos & Vasilopoulos 2018
XMMU J053108.3-690923	HMXRB	05:31:08	-69:09:24	50	Vasilopoulos et al. 2018; Maitra et al. 2021
XTE J1859+226	LMXRB	18:58:42	+22:39:29	6.3	Hameury et al. 2003; Gallo et al. 2008
GS 2023+338	LMXRB	20:24:04	+33:52:02	3.5	Kong et al. 2000
4U 1630-47	LMXRB	16:34:02	-47:23:35	10	Kong et al. 2000
CXOGLB J173617.6-444416	LMXRB	17:36:18	-44:44:17	9.9	Maxwell et al. 2012
CXOGLB J173616.9-444409	LMXRB	17:36:17	-44:44:10	9.9	Maxwell et al. 2012
CXOGLB J173617.3-444408	LMXRB	17:36:17	-44:44:08	9.9	Maxwell et al. 2012
CXOGLB J173618.1-444359	LMXRB	17:36:18	-44:43:59	9.9	Maxwell et al. 2012
CXOGLB J173617.5-444357	LMXRB	17:36:18	-44:43:57	9.9	Maxwell et al. 2012
IGR J17544-2619	HMXRB	17:54:25	-26:19:53	3.5, 3.6	in't Zand 2005; Sidoli et al. 2008
IGR J08408-4503	HMXRB	08:40:48	-45:03:32	2.7	Leyder et al. 2007
IGR J16479-4514	HMXRB	16:48:07	-45:12:07	4.9	Sidoli et al. 2008
XTE J1739-302	HMXRB	17:39:12	-30:20:38	2.7	Sidoli et al. 2008
IGR J18410-0535	HMXRB	18:41:00	-05:35:46	5	Sidoli et al. 2008
CI Cam <sup>c</sup>	ULX	04:19:42	+55:59:58	1-10	Bartlett et al. 2019

NOTE—Objects with light curves shown in the X-ray phase space are above the horizontal line. Below the line, we list objects for which we show the quiescent behavior. As with other variable phenomena that show recurrent outbursts and flares, some objects may correspond to a number of unique light curves.

<sup>a</sup>These data are not shared in the GitHub repository.

<sup>b</sup>The light curves *and* quiescent behavior of Aql X-1 and GX 339-4 are shown in the X-ray phase space.

<sup>c</sup>We note that CI Cam is a ULX as long as it is at a distance  $> 8$  kpc.

**Table A10.** Unclassified X-ray Sources

Name	RA	Dec	z	Distance (kpc)	Reference
XRT 000519	12:25:32	+13:03:59	0.23 - 1.5	$1.62 \times 10^4$ $1.1 \times 10^6$ $1.11 \times 10^7$	<a href="#">Jonker et al. 2013</a>
XRT 110103 <sup>a</sup>	14:08:29	-27:03:29	-	$9.49 \times 10^4$	<a href="#">Glennie et al. 2015</a>
XRT 120830 <sup>a</sup>	23:52:12	-46:43:43	-	0.08	<a href="#">Glennie et al. 2015</a>
Source 1	12:42:51	+02:38:35	-	$1.43 \times 10^4$	<a href="#">Irwin et al. 2016</a>
Source 2	13:25:53	-43:05:46	-	$3.8 \times 10^3$	<a href="#">Irwin et al. 2016</a>
CDF-S XT1 <sup>b</sup>	03:32:39	-27:51:34	0.3 - 2.23	$1.6 \times 10^6$ $1.81 \times 10^7$	<a href="#">Bauer et al. 2017</a>
CDF-S XT2	03:32:18	-27:52:24	0.738	$4.68 \times 10^6$	<a href="#">Xue et al. 2019</a>
EXMM 023135.0-603743	02:31:35	-60:37:43	0.092	$4.35 \times 10^5$	<a href="#">Novara et al. 2020</a>

<sup>a</sup>These data are digitized ([Rohatgi 2019](#)) and so are not included in the GitHub repository of light curves from this paper.

<sup>b</sup>See also [Quirola-Vásquez et al. \(2022, 2023\)](#) for data and analysis.

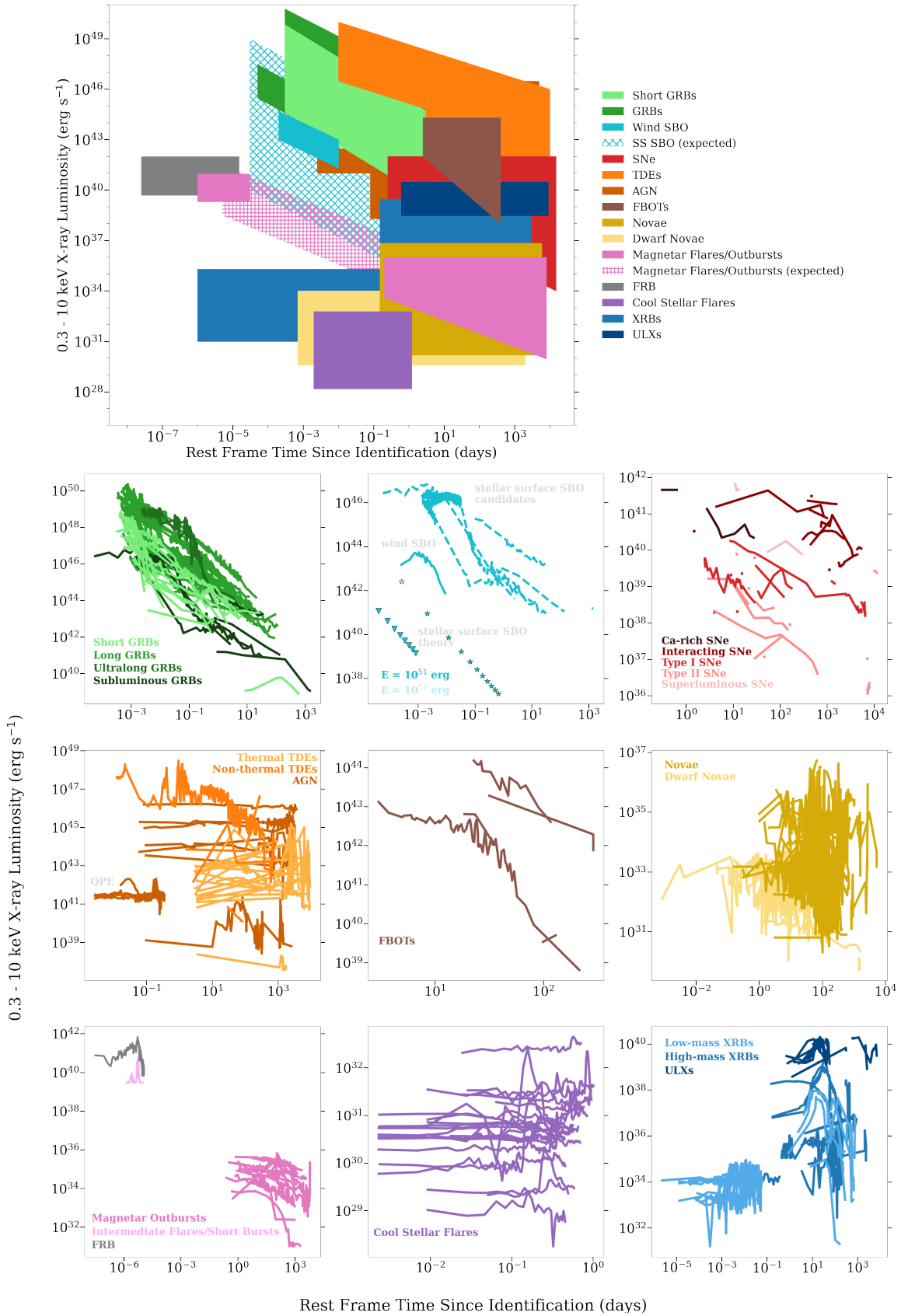


**Figure 12.** *Top:* A schematic illustration of the DLPS. Colored blocks cover the region where light curves of that class exist in the DLPS. The hatched blocks represent where we expect events of a particular class, but have a paucity of observations (for SBOs, we include in this the region of the DLPS where we have *candidate* stellar surface SBOs). *Bottom:* An additional view of the DLPS, which emphasizes the phase space of individual classes of transient rather than their position in the larger transient phase space. We note that the lower panels are all scaled individually in duration and luminosity.



## REFERENCES

- Abbott, B. P., Abbott, R., Abbott, T. D., et al. 2017, *ApJL*, 848, L12, doi: [10.3847/2041-8213/aa91c9](https://doi.org/10.3847/2041-8213/aa91c9)
- Alexander, K. D., van Velzen, S., Horesh, A., & Zauderer, B. A. 2020, *SSRv*, 216, 81, doi: [10.1007/s11214-020-00702-w](https://doi.org/10.1007/s11214-020-00702-w)
- Alp, D., & Larsson, J. 2020, *ApJ*, 896, 39, doi: [10.3847/1538-4357/ab91ba](https://doi.org/10.3847/1538-4357/ab91ba)
- Amati, L., O'Brien, P. T., Götz, D., et al. 2021, *Experimental Astronomy*, 52, 183, doi: [10.1007/s10686-021-09807-8](https://doi.org/10.1007/s10686-021-09807-8)
- Angelini, L., & Verbunt, F. 1989, *MNRAS*, 238, 697, doi: [10.1093/mnras/238.3.697](https://doi.org/10.1093/mnras/238.3.697)
- Arcavi, I., Wolf, W. M., Howell, D. A., et al. 2016, *ApJ*, 819, 35, doi: [10.3847/0004-637X/819/1/35](https://doi.org/10.3847/0004-637X/819/1/35)
- Arzoumanian, Z., Gendreau, K. C., Baker, C. L., et al. 2014, in *Society of Photo-Optical Instrumentation Engineers (SPIE) Conference Series*, Vol. 9144, *Space Telescopes and Instrumentation 2014: Ultraviolet to Gamma Ray*, ed. T. Takahashi, J.-W. A. den Herder, & M. Bautz, 914420, doi: [10.1117/12.2056811](https://doi.org/10.1117/12.2056811)
- Astropy Collaboration, Robitaille, T. P., Tollerud, E. J., et al. 2013, *A&A*, 558, A33, doi: [10.1051/0004-6361/201322068](https://doi.org/10.1051/0004-6361/201322068)
- Astropy Collaboration, Price-Whelan, A. M., Sipőcz, B. M., et al. 2018, *AJ*, 156, 123, doi: [10.3847/1538-3881/aabc4f](https://doi.org/10.3847/1538-3881/aabc4f)
- Auchettl, K., Guillochon, J., & Ramirez-Ruiz, E. 2017, *ApJ*, 838, 149, doi: [10.3847/1538-4357/aa633b](https://doi.org/10.3847/1538-4357/aa633b)
- Auchettl, K., Ramirez-Ruiz, E., & Guillochon, J. 2018, *ApJ*, 852, 37, doi: [10.3847/1538-4357/aa9b7c](https://doi.org/10.3847/1538-4357/aa9b7c)
- Aydi, E., Orio, M., Beardmore, A. P., et al. 2018, *MNRAS*, 480, 572, doi: [10.1093/mnras/sty1759](https://doi.org/10.1093/mnras/sty1759)
- Balberg, S., & Loeb, A. 2011, *MNRAS*, 414, 1715, doi: [10.1111/j.1365-2966.2011.18505.x](https://doi.org/10.1111/j.1365-2966.2011.18505.x)
- Barcons, X., Barret, D., Decourchelle, A., et al. 2012, *arXiv e-prints*, arXiv:1207.2745, <https://arxiv.org/abs/1207.2745>
- Bartlett, E. S., Clark, J. S., & Negueruela, I. 2019, *A&A*, 622, A93, doi: [10.1051/0004-6361/201834315](https://doi.org/10.1051/0004-6361/201834315)
- Bauer, F. E., Dwarkadas, V. V., Brandt, W. N., et al. 2008, *ApJ*, 688, 1210, doi: [10.1086/589761](https://doi.org/10.1086/589761)
- Bauer, F. E., Treister, E., Schawinski, K., et al. 2017, *Monthly Notices of the Royal Astronomical Society*, 467, 4841–4857, doi: [10.1093/mnras/stx417](https://doi.org/10.1093/mnras/stx417)
- Bietenholz, M. F., Bartel, N., Argo, M., et al. 2021, *ApJ*, 908, 75, doi: [10.3847/1538-4357/abccd9](https://doi.org/10.3847/1538-4357/abccd9)
- Bochenek, C. D., Ravi, V., Belov, K. V., et al. 2020, *Nature*, 587, 59, doi: [10.1038/s41586-020-2872-x](https://doi.org/10.1038/s41586-020-2872-x)
- Boella, G., Butler, R. C., Perola, G. C., et al. 1997, *A&AS*, 122, 299, doi: [10.1051/aas:1997136](https://doi.org/10.1051/aas:1997136)
- Bogdanov, S., Archibald, A. M., Bassa, C., et al. 2015, *ApJ*, 806, 148, doi: [10.1088/0004-637X/806/2/148](https://doi.org/10.1088/0004-637X/806/2/148)
- Boon, C. M., Bird, A. J., Coe, M. J., et al. 2017, *MNRAS*, 466, 1149, doi: [10.1093/mnras/stw3169](https://doi.org/10.1093/mnras/stw3169)
- Bose, S., Dong, S., Kochanek, C. S., et al. 2021, *MNRAS*, 503, 3472, doi: [10.1093/mnras/stab629](https://doi.org/10.1093/mnras/stab629)
- Brethauer, D., Margutti, R., Milisavljevic, D., et al. 2022, *arXiv e-prints*, arXiv:2206.00842, <https://arxiv.org/abs/2206.00842>
- Briel, U. G., Aschenbach, B., Hasinger, G., et al. 1996, *The ROSAT Users' Handbook*
- Bright, J. S., Fender, R. P., Motta, S. E., et al. 2018, *MNRAS*, 475, 4011, doi: [10.1093/mnras/sty077](https://doi.org/10.1093/mnras/sty077)
- Bright, J. S., Margutti, R., Matthews, D., et al. 2022, *ApJ*, 926, 112, doi: [10.3847/1538-4357/ac4506](https://doi.org/10.3847/1538-4357/ac4506)
- Brown, J. S., Holoiu, T. W. S., Auchettl, K., et al. 2017, *MNRAS*, 466, 4904, doi: [10.1093/mnras/stx033](https://doi.org/10.1093/mnras/stx033)
- Burrows, D. N., Hill, J. E., Nousek, J. A., et al. 2005, *SSRv*, 120, 165, doi: [10.1007/s11214-005-5097-2](https://doi.org/10.1007/s11214-005-5097-2)
- Byckling, K., Osborne, J. P., Wheatley, P. J., et al. 2009, *MNRAS*, 399, 1576, doi: [10.1111/j.1365-2966.2009.15378.x](https://doi.org/10.1111/j.1365-2966.2009.15378.x)
- Campana, S., Mangano, V., Blustin, A. J., et al. 2006, *Nature*, 442, 1008, doi: [10.1038/nature04892](https://doi.org/10.1038/nature04892)
- Carter, B., & Luminet, J. P. 1982, *Nature*, 296, 211, doi: [10.1038/296211a0](https://doi.org/10.1038/296211a0)
- . 1983, *A&A*, 121, 97
- Chakraborti, S., Ray, A., Smith, R., et al. 2013, *ApJ*, 774, 30, doi: [10.1088/0004-637X/774/1/30](https://doi.org/10.1088/0004-637X/774/1/30)
- . 2016, *ApJ*, 817, 22, doi: [10.3847/0004-637X/817/1/22](https://doi.org/10.3847/0004-637X/817/1/22)
- Chandra, P., Chevalier, R. A., Chugai, N., Fransson, C., & Soderberg, A. M. 2015, *The Astrophysical Journal*, 810, 32, doi: [10.1088/0004-637x/810/1/32](https://doi.org/10.1088/0004-637x/810/1/32)
- Chandra, P., Dwarkadas, V. V., Ray, A., Immler, S., & Pooley, D. 2009, *ApJ*, 699, 388, doi: [10.1088/0004-637X/699/1/388](https://doi.org/10.1088/0004-637X/699/1/388)
- Chandra X-ray Center, Chandra Project Science, MSFC, & Chandra IPI Teams. 2021, *The Chandra Proposers' Observatory Guide*, Tech. Rep. 24
- Chatzis, M., Petropoulou, M., & Vasilopoulos, G. 2022, *MNRAS*, 509, 2532, doi: [10.1093/mnras/stab3098](https://doi.org/10.1093/mnras/stab3098)
- Chen, G., Ravi, V., & Lu, W. 2020, *ApJ*, 897, 146, doi: [10.3847/1538-4357/ab982b](https://doi.org/10.3847/1538-4357/ab982b)
- Chesneau, O., Banerjee, D. P. K., Millour, F., et al. 2008, *A&A*, 487, 223, doi: [10.1051/0004-6361:200809485](https://doi.org/10.1051/0004-6361:200809485)
- Chevalier, R. A., & Fransson, C. 2017, in *Handbook of Supernovae*, ed. A. W. Alsabti & P. Murdin, 875, doi: [10.1007/978-3-319-21846-5\\_34](https://doi.org/10.1007/978-3-319-21846-5_34)

- Coppejans, D. L., Margutti, R., Terreran, G., et al. 2020, *ApJL*, 895, L23, doi: [10.3847/2041-8213/ab8cc7](https://doi.org/10.3847/2041-8213/ab8cc7)
- Corbel, S., Coriat, M., Brocksopp, C., et al. 2013, *MNRAS*, 428, 2500, doi: [10.1093/mnras/sts215](https://doi.org/10.1093/mnras/sts215)
- Coti Zelati, F., Rea, N., Pons, J. A., Campana, S., & Esposito, P. 2018, *MNRAS*, 474, 961, doi: [10.1093/mnras/stx2679](https://doi.org/10.1093/mnras/stx2679)
- Darnley, M. J., Ribeiro, V. A. R. M., Bode, M. F., & Munari, U. 2011, *A&A*, 530, A70, doi: [10.1051/0004-6361/201016038](https://doi.org/10.1051/0004-6361/201016038)
- De Luca, A., Salvaterra, R., Belfiore, A., et al. 2021, *A&A*, 650, A167, doi: [10.1051/0004-6361/202039783](https://doi.org/10.1051/0004-6361/202039783)
- de Ugarte Postigo, A., Izzo, L., Pugliese, G., et al. 2022, *GRB Coordinates Network*, 32748, 1
- Dong, F. A., & CHIME/FRB Collaboration. 2022, *The Astronomer's Telegram*, 15681, 1
- Drout, M. R., Chornock, R., Soderberg, A. M., et al. 2014, *ApJ*, 794, 23, doi: [10.1088/0004-637X/794/1/23](https://doi.org/10.1088/0004-637X/794/1/23)
- Dwarkadas, V. V., & Gruszko, J. 2012, *MNRAS*, 419, 1515, doi: [10.1111/j.1365-2966.2011.19808.x](https://doi.org/10.1111/j.1365-2966.2011.19808.x)
- Eappachen, D., Jonker, P. G., Fraser, M., et al. 2022, *MNRAS*, 514, 302, doi: [10.1093/mnras/stac1194](https://doi.org/10.1093/mnras/stac1194)
- Earnshaw, H. P., Heida, M., Brightman, M., et al. 2020, *ApJ*, 891, 153, doi: [10.3847/1538-4357/ab77b8](https://doi.org/10.3847/1538-4357/ab77b8)
- Eftekhari, T., Berger, E., Metzger, B. D., et al. 2022, *ApJ*, 935, 16, doi: [10.3847/1538-4357/ac7ce8](https://doi.org/10.3847/1538-4357/ac7ce8)
- Esposito, P., Rea, N., & Israel, G. L. 2021, in *Astrophysics and Space Science Library*, Vol. 461, *Astrophysics and Space Science Library*, ed. T. M. Belloni, M. Méndez, & C. Zhang, 97–142, doi: [10.1007/978-3-662-62110-3\\_3](https://doi.org/10.1007/978-3-662-62110-3_3)
- Esposito, P., De Luca, A., Turolla, R., et al. 2019, *A&A*, 626, A19, doi: [10.1051/0004-6361/201935412](https://doi.org/10.1051/0004-6361/201935412)
- Evans, P. A., Page, K. L., Beardmore, A. P., et al. 2022, *arXiv e-prints*, arXiv:2208.14478, <https://arxiv.org/abs/2208.14478>
- Evans, P. A., Beardmore, A. P., Page, K. L., et al. 2007, *A&A*, 469, 379, doi: [10.1051/0004-6361:20077530](https://doi.org/10.1051/0004-6361:20077530)
- . 2009, *MNRAS*, 397, 1177, doi: [10.1111/j.1365-2966.2009.14913.x](https://doi.org/10.1111/j.1365-2966.2009.14913.x)
- Evans, P. A., Page, K. L., Osborne, J. P., et al. 2020, *ApJS*, 247, 54, doi: [10.3847/1538-4365/ab7db9](https://doi.org/10.3847/1538-4365/ab7db9)
- Ferrigno, C., Bozzo, E., & Romano, P. 2022, *A&A*, 664, A99, doi: [10.1051/0004-6361/202243294](https://doi.org/10.1051/0004-6361/202243294)
- Fertig, D., Mukai, K., Nelson, T., & Cannizzo, J. K. 2011, *PASP*, 123, 1054, doi: [10.1086/661949](https://doi.org/10.1086/661949)
- Fong, W., Berger, E., Margutti, R., & Zauderer, B. A. 2015, *ApJ*, 815, 102, doi: [10.1088/0004-637X/815/2/102](https://doi.org/10.1088/0004-637X/815/2/102)
- Gallo, E., Homan, J., Jonker, P. G., & Tomsick, J. A. 2008, *ApJL*, 683, L51, doi: [10.1086/591230](https://doi.org/10.1086/591230)
- Ghirlanda, G., & Salvaterra, R. 2022, *ApJ*, 932, 10, doi: [10.3847/1538-4357/ac6e43](https://doi.org/10.3847/1538-4357/ac6e43)
- Giommi, P., Brandt, C. H., Barres de Almeida, U., et al. 2019, *A&A*, 631, A116, doi: [10.1051/0004-6361/201935646](https://doi.org/10.1051/0004-6361/201935646)
- Glennie, A., Jonker, P. G., Fender, R. P., Nagayama, T., & Pretorius, M. L. 2015, *Monthly Notices of the Royal Astronomical Society*, 450, 3765–3770, doi: [10.1093/mnras/stv801](https://doi.org/10.1093/mnras/stv801)
- Greiner, J., Voges, W., Boller, T., & Hartmann, D. 1999, *A&AS*, 138, 441, doi: [10.1051/aas:1999300](https://doi.org/10.1051/aas:1999300)
- Haberl, F., Geppert, U., Aschenbach, B., & Hasinger, G. 2006, *A&A*, 460, 811, doi: [10.1051/0004-6361:20066198](https://doi.org/10.1051/0004-6361:20066198)
- Haberl, F., & Sturm, R. 2016, *A&A*, 586, A81, doi: [10.1051/0004-6361/201527326](https://doi.org/10.1051/0004-6361/201527326)
- Hachisu, I., & Kato, M. 2018, *ApJS*, 237, 4, doi: [10.3847/1538-4365/aac833](https://doi.org/10.3847/1538-4365/aac833)
- Hajela, A., Margutti, R., Alexander, K. D., et al. 2019, *ApJL*, 886, L17, doi: [10.3847/2041-8213/ab5226](https://doi.org/10.3847/2041-8213/ab5226)
- Hajela, A., Margutti, R., Kathirgamaraju, A., et al. 2020, *Research Notes of the American Astronomical Society*, 4, 68, doi: [10.3847/2515-5172/ab9229](https://doi.org/10.3847/2515-5172/ab9229)
- Hameury, J. M., Barret, D., Lasota, J. P., et al. 2003, *A&A*, 399, 631, doi: [10.1051/0004-6361:20021746](https://doi.org/10.1051/0004-6361:20021746)
- Hancock, P. J., Anderson, G. E., Williams, A., et al. 2019, *PASA*, 36, e046, doi: [10.1017/pasa.2019.40](https://doi.org/10.1017/pasa.2019.40)
- Harris, C. R., Millman, K. J., van der Walt, S. J., et al. 2020, *Nature*, 585, 357, doi: [10.1038/s41586-020-2649-2](https://doi.org/10.1038/s41586-020-2649-2)
- Heinke, C. O., Bahramian, A., Degenaar, N., & Wijnands, R. 2015, *MNRAS*, 447, 3034, doi: [10.1093/mnras/stu2652](https://doi.org/10.1093/mnras/stu2652)
- Heng, K., Haberl, F., Aschenbach, B., & Hasinger, G. 2008, *ApJ*, 676, 361, doi: [10.1086/526517](https://doi.org/10.1086/526517)
- Ho, A. Y. Q., Perley, D. A., Gal-Yam, A., et al. 2021, *arXiv e-prints*, arXiv:2105.08811, <https://arxiv.org/abs/2105.08811>
- Ho, A. Y. Q., Margalit, B., Bremer, M., et al. 2022, *ApJ*, 932, 116, doi: [10.3847/1538-4357/ac4e97](https://doi.org/10.3847/1538-4357/ac4e97)
- Holoien, T. W. S., Brown, J. S., Auchettl, K., et al. 2018, *MNRAS*, 480, 5689, doi: [10.1093/mnras/sty2273](https://doi.org/10.1093/mnras/sty2273)
- Holoien, T. W. S., Valley, P. J., Auchettl, K., et al. 2019, *ApJ*, 883, 111, doi: [10.3847/1538-4357/ab3c66](https://doi.org/10.3847/1538-4357/ab3c66)
- Hunter, J. D. 2007, *Computing in Science & Engineering*, 9, 90, doi: [10.1109/MCSE.2007.55](https://doi.org/10.1109/MCSE.2007.55)
- Hurley, K., Boggs, S. E., Smith, D. M., et al. 2005, *Nature*, 434, 1098, doi: [10.1038/nature03519](https://doi.org/10.1038/nature03519)
- Immler, S. 2010, *The Astronomer's Telegram*, 2478, 1
- Immler, S., Brown, P. J., Filippenko, A. V., & Pooley, D. 2007a, *The Astronomer's Telegram*, 1290, 1
- Immler, S., Li, B., Yang, Y., & Wilson, A. 2007b, *Central Bureau Electronic Telegrams*, 828, 1

- Immler, S., Milne, P., & Pooley, D. 2010, *The Astronomer's Telegram*, 3012, 1
- Immler, S., & Pooley, D. 2007, *The Astronomer's Telegram*, 1004, 1
- Immler, S., Pooley, D., & Brown, P. J. 2007c, *The Astronomer's Telegram*, 981, 1
- Immler, S., Pooley, D., Brown, P. J., Li, W., & Filippenko, A. V. 2007d, *The Astronomer's Telegram*, 1284, 1
- Immler, S., Pooley, D., Brown, P. J., & Milne, P. 2009, *The Astronomer's Telegram*, 1918, 1
- Immler, S., & Russell, B. R. 2009, *The Astronomer's Telegram*, 2111, 1
- Immler, S., Brown, P. J., Milne, P., et al. 2007e, *ApJ*, 664, 435, doi: [10.1086/518466](https://doi.org/10.1086/518466)
- Immler, S., Modjaz, M., Landsman, W., et al. 2008, *ApJL*, 674, L85, doi: [10.1086/529373](https://doi.org/10.1086/529373)
- in't Zand, J. J. M. 2005, *A&A*, 441, L1, doi: [10.1051/0004-6361:200500162](https://doi.org/10.1051/0004-6361:200500162)
- Irwin, C. M., Linial, I., Nakar, E., Piran, T., & Sari, R. 2021, *MNRAS*, 508, 5766, doi: [10.1093/mnras/stab2705](https://doi.org/10.1093/mnras/stab2705)
- Irwin, J. A., Maksym, W. P., Sivakoff, G. R., et al. 2016, *Nature*, 538, 356, doi: [10.1038/nature19822](https://doi.org/10.1038/nature19822)
- Israel, G. L., Romano, P., Mangano, V., et al. 2008, *ApJ*, 685, 1114, doi: [10.1086/590486](https://doi.org/10.1086/590486)
- Jacobson-Galán, W. V., Margutti, R., Kilpatrick, C. D., et al. 2020, *ApJ*, 898, 166, doi: [10.3847/1538-4357/ab9e66](https://doi.org/10.3847/1538-4357/ab9e66)
- Jacobson-Galán, W. V., Venkatraman, P., Margutti, R., et al. 2022, *ApJ*, 932, 58, doi: [10.3847/1538-4357/ac67dc](https://doi.org/10.3847/1538-4357/ac67dc)
- Jahoda, K., Swank, J. H., Giles, A. B., et al. 1996, in *Society of Photo-Optical Instrumentation Engineers (SPIE) Conference Series*, Vol. 2808, EUV, X-Ray, and Gamma-Ray Instrumentation for Astronomy VII, ed. O. H. Siegmund & M. A. Gummin, 59–70, doi: [10.1117/12.256034](https://doi.org/10.1117/12.256034)
- Jansen, F., Lumb, D., Altieri, B., et al. 2001, *A&A*, 365, L1, doi: [10.1051/0004-6361:20000036](https://doi.org/10.1051/0004-6361:20000036)
- Jonker, P. G., Miller-Jones, J. C. A., Homan, J., et al. 2012, *MNRAS*, 423, 3308, doi: [10.1111/j.1365-2966.2012.21116.x](https://doi.org/10.1111/j.1365-2966.2012.21116.x)
- Jonker, P. G., Glennie, A., Heida, M., et al. 2013, *The Astrophysical Journal*, 779, 14, doi: [10.1088/0004-637x/779/1/14](https://doi.org/10.1088/0004-637x/779/1/14)
- Kantharia, N. G. 2017, arXiv e-prints, arXiv:1703.04087, <https://arxiv.org/abs/1703.04087>
- Koliopanos, F., & Vasilopoulos, G. 2018, *A&A*, 614, A23, doi: [10.1051/0004-6361/201731623](https://doi.org/10.1051/0004-6361/201731623)
- Komossa, S. 2015, *Journal of High Energy Astrophysics*, 7, 148, doi: [10.1016/j.jheap.2015.04.006](https://doi.org/10.1016/j.jheap.2015.04.006)
- Kong, A. K. H., Kuulkers, E., Charles, P. A., & Homer, L. 2000, *MNRAS*, 312, L49, doi: [10.1046/j.1365-8711.2000.03334.x](https://doi.org/10.1046/j.1365-8711.2000.03334.x)
- Kouveliotou, C., Meegan, C. A., Fishman, G. J., et al. 1993, *ApJL*, 413, L101, doi: [10.1086/186969](https://doi.org/10.1086/186969)
- Kouveliotou, C., Woosley, S. E., Patel, S. K., et al. 2004, *ApJ*, 608, 872, doi: [10.1086/420878](https://doi.org/10.1086/420878)
- Kulkarni, S. R. 2012, arXiv e-prints, arXiv:1202.2381, <https://arxiv.org/abs/1202.2381>
- La Palombara, N., & Mereghetti, S. 2007, *A&A*, 474, 137, doi: [10.1051/0004-6361:20077970](https://doi.org/10.1051/0004-6361:20077970)
- Levan, A. J., Tanvir, N. R., Starling, R. L. C., et al. 2014, *ApJ*, 781, 13, doi: [10.1088/0004-637X/781/1/13](https://doi.org/10.1088/0004-637X/781/1/13)
- Leyder, J. C., Walter, R., Lazos, M., Masetti, N., & Produit, N. 2007, *A&A*, 465, L35, doi: [10.1051/0004-6361:20066317](https://doi.org/10.1051/0004-6361:20066317)
- Li, C. K., Lin, L., Xiong, S. L., et al. 2021, *Nature Astronomy*, 5, 378, doi: [10.1038/s41550-021-01302-6](https://doi.org/10.1038/s41550-021-01302-6)
- Li, K.-L., Hamsch, F.-J., Munari, U., et al. 2020a, *ApJ*, 905, 114, doi: [10.3847/1538-4357/abc3be](https://doi.org/10.3847/1538-4357/abc3be)
- Li, K. L., & Pun, C. S. J. 2011, arXiv e-prints, arXiv:1109.0981, doi: [10.48550/arXiv.1109.0981](https://doi.org/10.48550/arXiv.1109.0981)
- Li, X., Li, X., Tan, Y., et al. 2020b, *Journal of High Energy Astrophysics*, 27, 64, doi: [10.1016/j.jheap.2020.02.009](https://doi.org/10.1016/j.jheap.2020.02.009)
- Linford, J. D., Chomiuk, L., Nelson, T., et al. 2017, *ApJ*, 842, 73, doi: [10.3847/1538-4357/aa7512](https://doi.org/10.3847/1538-4357/aa7512)
- López-Navas, E., Degenaar, N., Parikh, A. S., Hernández Santisteban, J. V., & van den Eijnden, J. 2020, *MNRAS*, 493, 940, doi: [10.1093/mnras/staa275](https://doi.org/10.1093/mnras/staa275)
- Lorimer, D. R., Bailes, M., McLaughlin, M. A., Narkevic, D. J., & Crawford, F. 2007, *Science*, 318, 777, doi: [10.1126/science.1147532](https://doi.org/10.1126/science.1147532)
- Lutovinov, A. A., Tsygankov, S. S., Krivonos, R. A., Molkov, S. V., & Poutanen, J. 2017, *ApJ*, 834, 209, doi: [10.3847/1538-4357/834/2/209](https://doi.org/10.3847/1538-4357/834/2/209)
- Maitra, C., Haberl, F., Vasilopoulos, G., et al. 2021, *A&A*, 647, A8, doi: [10.1051/0004-6361/202039468](https://doi.org/10.1051/0004-6361/202039468)
- Mangano, V., Burrows, D. N., Sbarufatti, B., & Cannizzo, J. K. 2016, *ApJ*, 817, 103, doi: [10.3847/0004-637X/817/2/103](https://doi.org/10.3847/0004-637X/817/2/103)
- Margutti, R., & Chornock, R. 2021, *ARA&A*, 59, doi: [10.1146/annurev-astro-112420-030742](https://doi.org/10.1146/annurev-astro-112420-030742)
- Margutti, R., Soderberg, A., & Milisavljevic, D. 2013, *The Astronomer's Telegram*, 5106, 1
- Margutti, R., Metzger, B. D., Chornock, R., et al. 2019, *The Astrophysical Journal*, 872, 18, doi: [10.3847/1538-4357/aafa01](https://doi.org/10.3847/1538-4357/aafa01)
- Matsuoka, M., Kawasaki, K., Ueno, S., et al. 2009, *PASJ*, 61, 999, doi: [10.1093/pasj/61.5.999](https://doi.org/10.1093/pasj/61.5.999)

- Matthews, D., Brethauer, D., Margutti, R., et al. 2022, *Transient Name Server AstroNote*, 218, 1
- Matthews, D., & Margutti, R. 2023, *Transient Name Server AstroNote*, 159, 1
- Maxwell, J. E., Lugger, P. M., Cohn, H. N., et al. 2012, *ApJ*, 756, 147, doi: [10.1088/0004-637X/756/2/147](https://doi.org/10.1088/0004-637X/756/2/147)
- Mazzali, P. A., Valenti, S., Della Valle, M., et al. 2008, *Science*, 321, 1185, doi: [10.1126/science.1158088](https://doi.org/10.1126/science.1158088)
- McGowan, K. E., Priedhorsky, W. C., & Trudolyubov, S. P. 2004, *ApJ*, 601, 1100, doi: [10.1086/380758](https://doi.org/10.1086/380758)
- Meidinger, N. 2018, *Contributions of the Astronomical Observatory Skalnaté Pleso*, 48, 498.  
<https://arxiv.org/abs/1702.01079>
- Mereghetti, S., Savchenko, V., Ferrigno, C., et al. 2020, *ApJL*, 898, L29, doi: [10.3847/2041-8213/aba2cf](https://doi.org/10.3847/2041-8213/aba2cf)
- Merloni, A., Predehl, P., Becker, W., et al. 2012, arXiv e-prints, arXiv:1209.3114.  
<https://arxiv.org/abs/1209.3114>
- Metzger, B. D., Williams, P. K. G., & Berger, E. 2015, *ApJ*, 806, 224, doi: [10.1088/0004-637X/806/2/224](https://doi.org/10.1088/0004-637X/806/2/224)
- Middleton, M. J., Miller-Jones, J. C. A., Markoff, S., et al. 2013, *Nature*, 493, 187, doi: [10.1038/nature11697](https://doi.org/10.1038/nature11697)
- Miller, J. M., Kaastra, J. S., Miller, M. C., et al. 2015, *Nature*, 526, 542, doi: [10.1038/nature15708](https://doi.org/10.1038/nature15708)
- Miniutti, G., Saxton, R. D., Giustini, M., et al. 2019, *Nature*, 573, 381, doi: [10.1038/s41586-019-1556-x](https://doi.org/10.1038/s41586-019-1556-x)
- Misra, K., Pooley, D., Chandra, P., et al. 2007, *MNRAS*, 381, 280, doi: [10.1111/j.1365-2966.2007.12258.x](https://doi.org/10.1111/j.1365-2966.2007.12258.x)
- Miura, J., Tsujimoto, M., Tsuboi, Y., et al. 2008, *PASJ*, 60, S49, doi: [10.1093/pasj/60.sp1.S49](https://doi.org/10.1093/pasj/60.sp1.S49)
- Mong, Y.-L., & Ng, C.-Y. 2018, *The Astrophysical Journal*, 852, 86, doi: [10.3847/1538-4357/aa9e90](https://doi.org/10.3847/1538-4357/aa9e90)
- Mukai, K. 1993, *Legacy*, 3, 21
- . 2017, *PASP*, 129, 062001, doi: [10.1088/1538-3873/aa6736](https://doi.org/10.1088/1538-3873/aa6736)
- Mukai, K., Orío, M., & Della Valle, M. 2008, *ApJ*, 677, 1248, doi: [10.1086/529362](https://doi.org/10.1086/529362)
- Munari, U., Ribeiro, V. A. R. M., Bode, M. F., & Saguner, T. 2011, *MNRAS*, 410, 525, doi: [10.1111/j.1365-2966.2010.17462.x](https://doi.org/10.1111/j.1365-2966.2010.17462.x)
- Mushotzky, R. 2018, in *Society of Photo-Optical Instrumentation Engineers (SPIE) Conference Series*, Vol. 10699, *Space Telescopes and Instrumentation 2018: Ultraviolet to Gamma Ray*, ed. J.-W. A. den Herder, S. Nikzad, & K. Nakazawa, 1069929, doi: [10.1117/12.2310003](https://doi.org/10.1117/12.2310003)
- Nakar, E. 2015, *ApJ*, 807, 172, doi: [10.1088/0004-637X/807/2/172](https://doi.org/10.1088/0004-637X/807/2/172)
- . 2020, *PhR*, 886, 1, doi: [10.1016/j.physrep.2020.08.008](https://doi.org/10.1016/j.physrep.2020.08.008)
- Nakar, E., & Sari, R. 2010, *ApJ*, 725, 904, doi: [10.1088/0004-637X/725/1/904](https://doi.org/10.1088/0004-637X/725/1/904)
- . 2012, *ApJ*, 747, 88, doi: [10.1088/0004-637X/747/2/88](https://doi.org/10.1088/0004-637X/747/2/88)
- Neustroev, V. V., Page, K. L., Kuulkers, E., et al. 2018, *A&A*, 611, A13, doi: [10.1051/0004-6361/201731719](https://doi.org/10.1051/0004-6361/201731719)
- Nisenoff, A., Dwarkadas, V. V., & Ross, M. C. 2020, *Research Notes of the American Astronomical Society*, 4, 195, doi: [10.3847/2515-5172/abc6a7](https://doi.org/10.3847/2515-5172/abc6a7)
- Norris, J. P. 2003, in *American Institute of Physics Conference Series*, Vol. 686, *The Astrophysics of Gravitational Wave Sources*, ed. J. M. Centrella, 74–83, doi: [10.1063/1.1629417](https://doi.org/10.1063/1.1629417)
- Novara, G., Esposito, P., Tiengo, A., et al. 2020, *ApJ*, 898, 37, doi: [10.3847/1538-4357/ab98f8](https://doi.org/10.3847/1538-4357/ab98f8)
- O’Brien, P. T., & Smartt, S. J. 2013, *Philosophical Transactions of the Royal Society of London Series A*, 371, 20120498, doi: [10.1098/rsta.2012.0498](https://doi.org/10.1098/rsta.2012.0498)
- Olausen, S. A., & Kaspi, V. M. 2014, *The Astrophysical Journal Supplement Series*, 212, 6, doi: [10.1088/0067-0049/212/1/6](https://doi.org/10.1088/0067-0049/212/1/6)
- Page, K. L., Beardmore, A. P., & Osborne, J. P. 2020, *Advances in Space Research*, 66, 1169, doi: [10.1016/j.asr.2019.08.003](https://doi.org/10.1016/j.asr.2019.08.003)
- Pala, A. F., Gänsicke, B. T., Breedt, E., et al. 2020, *MNRAS*, 494, 3799, doi: [10.1093/mnras/staa764](https://doi.org/10.1093/mnras/staa764)
- pandas development team, T. 2020, *pandas-dev/pandas: Pandas, 1.1.3*, Zenodo, doi: [10.5281/zenodo.4067057](https://doi.org/10.5281/zenodo.4067057)
- Pedregosa, F., Varoquaux, G., Gramfort, A., et al. 2011, *Journal of Machine Learning Research*, 12, 2825
- Petroff, E., Hessels, J. W. T., & Lorimer, D. R. 2019, *A&A Rv*, 27, 4, doi: [10.1007/s00159-019-0116-6](https://doi.org/10.1007/s00159-019-0116-6)
- . 2022, *A&A Rv*, 30, 2, doi: [10.1007/s00159-022-00139-w](https://doi.org/10.1007/s00159-022-00139-w)
- Pian, E., Amati, L., Antonelli, L. A., et al. 2000, *ApJ*, 536, 778, doi: [10.1086/308978](https://doi.org/10.1086/308978)
- Pietka, M., Fender, R. P., & Keane, E. F. 2015, *MNRAS*, 446, 3687, doi: [10.1093/mnras/stu2335](https://doi.org/10.1093/mnras/stu2335)
- Pietrzyński, G., Graczyk, D., Gieren, W., et al. 2013, *Nature*, 495, 76, doi: [10.1038/nature11878](https://doi.org/10.1038/nature11878)
- Pleunis, Z., Good, D. C., Kaspi, V. M., et al. 2021, *ApJ*, 923, 1, doi: [10.3847/1538-4357/ac33ac](https://doi.org/10.3847/1538-4357/ac33ac)
- Poggiani, R. 2009, *NewA*, 14, 4, doi: [10.1016/j.newast.2008.04.004](https://doi.org/10.1016/j.newast.2008.04.004)
- Pooley, D., Immler, S., & Filippenko, A. V. 2007, *The Astronomer’s Telegram*, 1023, 1
- Pooley, D., Lewin, W. H. G., Fox, D. W., et al. 2002, *ApJ*, 572, 932, doi: [10.1086/340346](https://doi.org/10.1086/340346)
- Predehl, P., Andritschke, R., Arefiev, V., et al. 2021, *A&A*, 647, A1, doi: [10.1051/0004-6361/202039313](https://doi.org/10.1051/0004-6361/202039313)
- Pursiainen, M., Childress, M., Smith, M., et al. 2018, *MNRAS*, 481, 894, doi: [10.1093/mnras/sty2309](https://doi.org/10.1093/mnras/sty2309)

- Pye, J. P., Rosen, S., Fyfe, D., & Schröder, A. C. 2015, *A&A*, 581, A28, doi: [10.1051/0004-6361/201526217](https://doi.org/10.1051/0004-6361/201526217)
- Qiu, Y., Soria, R., Wang, S., et al. 2019, *ApJ*, 877, 57, doi: [10.3847/1538-4357/ab16e7](https://doi.org/10.3847/1538-4357/ab16e7)
- Quirola-Vásquez, J., Bauer, F. E., Jonker, P. G., et al. 2022, *A&A*, 663, A168, doi: [10.1051/0004-6361/202243047](https://doi.org/10.1051/0004-6361/202243047)
- . 2023, arXiv e-prints, arXiv:2304.13795, doi: [10.48550/arXiv.2304.13795](https://doi.org/10.48550/arXiv.2304.13795)
- Raj, A., Banerjee, D. P. K., & Ashok, N. M. 2013, *MNRAS*, 433, 2657, doi: [10.1093/mnras/stt946](https://doi.org/10.1093/mnras/stt946)
- Raj, A., Ashok, N. M., Rudy, R. J., et al. 2015, *AJ*, 149, 136, doi: [10.1088/0004-6256/149/4/136](https://doi.org/10.1088/0004-6256/149/4/136)
- Ramsden, P., Lanning, D., Nicholl, M., & McGee, S. L. 2022, *MNRAS*, 515, 1146, doi: [10.1093/mnras/stac1810](https://doi.org/10.1093/mnras/stac1810)
- Ray, P. S., Arzoumanian, Z., Ballantyne, D., et al. 2019, arXiv e-prints, arXiv:1903.03035, <https://arxiv.org/abs/1903.03035>
- Rea, N., Borghese, A., Esposito, P., et al. 2016, *ApJL*, 828, L13, doi: [10.3847/2041-8205/828/1/L13](https://doi.org/10.3847/2041-8205/828/1/L13)
- Rea, N., Esposito, P., Pons, J. A., et al. 2013, *ApJL*, 775, L34, doi: [10.1088/2041-8205/775/2/L34](https://doi.org/10.1088/2041-8205/775/2/L34)
- Reig, P. 2011, *Ap&SS*, 332, 1, doi: [10.1007/s10509-010-0575-8](https://doi.org/10.1007/s10509-010-0575-8)
- Rivera Sandoval, L. E., Maccarone, T. J., Corsi, A., et al. 2018, *MNRAS*, 480, L146, doi: [10.1093/mnrasl/sly145](https://doi.org/10.1093/mnrasl/sly145)
- . 2019, *MNRAS*, 484, L7, doi: [10.1093/mnrasl/sly235](https://doi.org/10.1093/mnrasl/sly235)
- Rohatgi, A. 2019, *WebPlotDigitizer* (4.2), <https://automeris.io/WebPlotDigitizer>
- Roming, P. W. A., Pritchard, T. A., Brown, P. J., et al. 2009, *ApJL*, 704, L118, doi: [10.1088/0004-637X/704/2/L118](https://doi.org/10.1088/0004-637X/704/2/L118)
- Ross, M., & Dwarkadas, V. V. 2017, *AJ*, 153, 246, doi: [10.3847/1538-3881/aa6d50](https://doi.org/10.3847/1538-3881/aa6d50)
- Rouco Escorial, A., Fong, W.-f., Berger, E., et al. 2022, arXiv e-prints, arXiv:2210.05695, <https://arxiv.org/abs/2210.05695>
- Russell, B. R., & Immler, S. 2010, *The Astronomer's Telegram*, 2389, 1
- Russell, B. R., Immler, S., & Milne, P. 2010, *The Astronomer's Telegram*, 2618, 1
- Russell, T. D., Miller-Jones, J. C. A., Sivakoff, G. R., et al. 2016, *MNRAS*, 460, 3720, doi: [10.1093/mnras/stw1238](https://doi.org/10.1093/mnras/stw1238)
- Sazonov, S., Gilfanov, M., Medvedev, P., et al. 2021, *MNRAS*, 508, 3820, doi: [10.1093/mnras/stab2843](https://doi.org/10.1093/mnras/stab2843)
- Sazonov, S. Y., Lutovinov, A. A., & Sunyaev, R. A. 2004, *Nature*, 430, 646, doi: [10.1038/nature02748](https://doi.org/10.1038/nature02748)
- Schaefer, B. E. 2010, *ApJS*, 187, 275, doi: [10.1088/0067-0049/187/2/275](https://doi.org/10.1088/0067-0049/187/2/275)
- . 2018, *MNRAS*, 481, 3033, doi: [10.1093/mnras/sty2388](https://doi.org/10.1093/mnras/sty2388)
- Schlegel, E. M. 2001, *ApJL*, 556, L25, doi: [10.1086/322269](https://doi.org/10.1086/322269)
- Schlegel, E. M., & Ryder, S. 2002, *IAUC*, 7913, 1
- Schulze, S., Ho, A. Y. Q., Perley, D. A., Yan, L., & Fremling, C. 2022, *Transient Name Server AstroNote*, 207, 1
- Sidoli, L., Romano, P., Mangano, V., et al. 2008, *ApJ*, 687, 1230, doi: [10.1086/590077](https://doi.org/10.1086/590077)
- Soderberg, A., Grindlay, J. E., Bloom, J. S., et al. 2009, in *astro2010: The Astronomy and Astrophysics Decadal Survey*, Vol. 2010, 278. <https://arxiv.org/abs/0902.3674>
- Soderberg, A. M., Chevalier, R. A., Kulkarni, S. R., & Frail, D. A. 2006, *ApJ*, 651, 1005, doi: [10.1086/507571](https://doi.org/10.1086/507571)
- Soderberg, A. M., Berger, E., Page, K. L., et al. 2008, *Nature*, 453, 469, doi: [10.1038/nature06997](https://doi.org/10.1038/nature06997)
- Soderberg, A. M., Margutti, R., Zauderer, B. A., et al. 2012, *ApJ*, 752, 78, doi: [10.1088/0004-637X/752/2/78](https://doi.org/10.1088/0004-637X/752/2/78)
- Soria, R., Pian, E., & Mazzali, P. A. 2004, *A&A*, 413, 107, doi: [10.1051/0004-6361:20031506](https://doi.org/10.1051/0004-6361:20031506)
- Staley, T. D., Titterton, D. J., Fender, R. P., et al. 2013, *MNRAS*, 428, 3114, doi: [10.1093/mnras/sts259](https://doi.org/10.1093/mnras/sts259)
- Stone, N. C., & Metzger, B. D. 2016, *MNRAS*, 455, 859, doi: [10.1093/mnras/stv2281](https://doi.org/10.1093/mnras/stv2281)
- Sturm, R., Haberl, F., Aschenbach, B., & Hasinger, G. 2010, *A&A*, 515, A5, doi: [10.1051/0004-6361/200913317](https://doi.org/10.1051/0004-6361/200913317)
- Sugawara, Y., Nakahira, S., Negoro, H., et al. 2020, *GRB Coordinates Network*, 27661, 1
- Sugizaki, M. 2010, in *The First Year of MAXI: Monitoring Variable X-ray Sources*, 14
- Svirski, G., & Nakar, E. 2014, *ApJL*, 788, L14, doi: [10.1088/2041-8205/788/1/L14](https://doi.org/10.1088/2041-8205/788/1/L14)
- Tanaka, M., Tominaga, N., Morokuma, T., et al. 2016, *ApJ*, 819, 5, doi: [10.3847/0004-637X/819/1/5](https://doi.org/10.3847/0004-637X/819/1/5)
- Tanaka, Y., Inoue, H., & Holt, S. S. 1994, *PASJ*, 46, L37
- Tetarenko, B. E., Sivakoff, G. R., Heinke, C. O., & Gladstone, J. C. 2016, *ApJS*, 222, 15, doi: [10.3847/0067-0049/222/2/15](https://doi.org/10.3847/0067-0049/222/2/15)
- The CHIME/FRB Collaboration, Andersen, B. Å. C., Bandura, K. Å. M., Bhardwaj, M., et al. 2020, *Nature*, 587, 54, doi: [10.1038/s41586-020-2863-y](https://doi.org/10.1038/s41586-020-2863-y)
- The Lynx Team. 2019, *Lynx X-ray Observatory Concept Study Report*, Tech. rep., Lynx Observatory
- Tozzi, P., Gilli, R., Mainieri, V., et al. 2006, *A&A*, 451, 457, doi: [10.1051/0004-6361:20042592](https://doi.org/10.1051/0004-6361:20042592)
- Trümper, J. 1990, *International Astronomical Union Colloquium*, 115, 291–294, doi: [10.1017/S0252921100012483](https://doi.org/10.1017/S0252921100012483)
- Tsuboi, Y., Yamazaki, K., Sugawara, Y., et al. 2016, *PASJ*, 68, 90, doi: [10.1093/pasj/psw081](https://doi.org/10.1093/pasj/psw081)
- Tsunemi, H., Tomida, H., Katayama, H., et al. 2010, *Publications of the Astronomical Society of Japan*, 62, 1371, doi: [10.1093/pasj/62.6.1371](https://doi.org/10.1093/pasj/62.6.1371)

- Vasilopoulos, G., Haberl, F., & Maggi, P. 2017a, MNRAS, 470, 1971, doi: [10.1093/mnras/stx1359](https://doi.org/10.1093/mnras/stx1359)
- Vasilopoulos, G., Haberl, F., Sturm, R., Maggi, P., & Udalski, A. 2014, A&A, 567, A129, doi: [10.1051/0004-6361/201423934](https://doi.org/10.1051/0004-6361/201423934)
- Vasilopoulos, G., Lander, S. K., Koliopanos, F., & Bailyn, C. D. 2020a, MNRAS, 491, 4949, doi: [10.1093/mnras/stz3298](https://doi.org/10.1093/mnras/stz3298)
- Vasilopoulos, G., Maitra, C., Haberl, F., Hatzidimitriou, D., & Petropoulou, M. 2018, MNRAS, 475, 220, doi: [10.1093/mnras/stx3139](https://doi.org/10.1093/mnras/stx3139)
- Vasilopoulos, G., Zezas, A., Antoniou, V., & Haberl, F. 2017b, MNRAS, 470, 4354, doi: [10.1093/mnras/stx1507](https://doi.org/10.1093/mnras/stx1507)
- Vasilopoulos, G., Ray, P. S., Gendreau, K. C., et al. 2020b, MNRAS, 494, 5350, doi: [10.1093/mnras/staa991](https://doi.org/10.1093/mnras/staa991)
- Villar, V. A., Berger, E., Metzger, B. D., & Guillochon, J. 2017, ApJ, 849, 70, doi: [10.3847/1538-4357/aa8fcb](https://doi.org/10.3847/1538-4357/aa8fcb)
- Virtanen, P., Gommers, R., Oliphant, T. E., et al. 2020, Nature Methods, 17, 261, doi: [10.1038/s41592-019-0686-2](https://doi.org/10.1038/s41592-019-0686-2)
- Wang, C. W., Xiong, S. L., Zhang, Y. Q., et al. 2022, The Astronomer's Telegram, 15682, 1
- Watson, D., Hjorth, J., Levan, A., et al. 2004, ApJL, 605, L101, doi: [10.1086/420844](https://doi.org/10.1086/420844)
- Watson, M. G., Auguères, J. L., Ballet, J., et al. 2001, A&A, 365, L51, doi: [10.1051/0004-6361:20000067](https://doi.org/10.1051/0004-6361:20000067)
- Wei, J., Cordier, B., Antier, S., et al. 2016, arXiv e-prints, arXiv:1610.06892. <https://arxiv.org/abs/1610.06892>
- Weisskopf, M. C., Tananbaum, H. D., Van Speybroeck, L. P., & O'Dell, S. L. 2000, in Society of Photo-Optical Instrumentation Engineers (SPIE) Conference Series, Vol. 4012, X-Ray Optics, Instruments, and Missions III, ed. J. E. Truemper & B. Aschenbach, 2–16, doi: [10.1117/12.391545](https://doi.org/10.1117/12.391545)
- Wes McKinney. 2010, in Proceedings of the 9th Python in Science Conference, ed. Stéfan van der Walt & Jarrod Millman, 56 – 61, doi: [10.25080/Majora-92bf1922-00a](https://doi.org/10.25080/Majora-92bf1922-00a)
- Wheatley, P. J., Mauche, C. W., & Mattei, J. A. 2003, MNRAS, 345, 49, doi: [10.1046/j.1365-8711.2003.06936.x](https://doi.org/10.1046/j.1365-8711.2003.06936.x)
- Wilson-Hodge, C. A., Malacaria, C., Jenke, P. A., et al. 2018, ApJ, 863, 9, doi: [10.3847/1538-4357/aace60](https://doi.org/10.3847/1538-4357/aace60)
- Worpel, H., Schwöpe, A. D., Traulsen, I., Mukai, K., & Ok, S. 2020, A&A, 639, A17, doi: [10.1051/0004-6361/202038038](https://doi.org/10.1051/0004-6361/202038038)
- Xue, Y. Q., Zheng, X. C., Li, Y., et al. 2019, Nature, 568, 198, doi: [10.1038/s41586-019-1079-5](https://doi.org/10.1038/s41586-019-1079-5)
- Yao, Y., Ho, A. Y. Q., Medvedev, P., et al. 2022, ApJ, 934, 104, doi: [10.3847/1538-4357/ac7a41](https://doi.org/10.3847/1538-4357/ac7a41)
- Yao, Y., Ravi, V., Gezari, S., et al. 2023, arXiv e-prints, arXiv:2303.06523, doi: [10.48550/arXiv.2303.06523](https://doi.org/10.48550/arXiv.2303.06523)
- Yuan, W. 2017, in 7 years of MAXI: monitoring X-ray Transients, ed. M. Serino, M. Shidatsu, W. Iwakiri, & T. Mihara, 247
- Zampieri, L., Mucciarelli, P., Pastorello, A., et al. 2005, MNRAS, 364, 1419, doi: [10.1111/j.1365-2966.2005.09671.x](https://doi.org/10.1111/j.1365-2966.2005.09671.x)
- Zhang, S., Santangelo, A., Feroci, M., et al. 2019, Science China Physics, Mechanics, and Astronomy, 62, 29502, doi: [10.1007/s11433-018-9309-2](https://doi.org/10.1007/s11433-018-9309-2)
- Zhang, S.-N., Li, T., Lu, F., et al. 2020, Science China Physics, Mechanics, and Astronomy, 63, 249502, doi: [10.1007/s11433-019-1432-6](https://doi.org/10.1007/s11433-019-1432-6)